Title

DEVELOPMENT OF A CCD CAMERA FOR AN AUTOMATED SUPERNOVA SEARCH AND OBSERVATIONS OF A SUPERNOVA IN NGC 5033

Author

Burns, M.S.

Publication Date

1985-11-01

Lawrence Berkeley Laboratory

UNIVERSITY OF CALIFORNIA

Physics Division

DEVELOPMENT OF A CCD CAMERA FOR AN AUTOMATED SUPERNOVA SEARCH AND OBSERVATIONS OF A SUPERNOVA IN NGC 5033

M.S. Burns
(Ph.D. Thesis)

November 1985

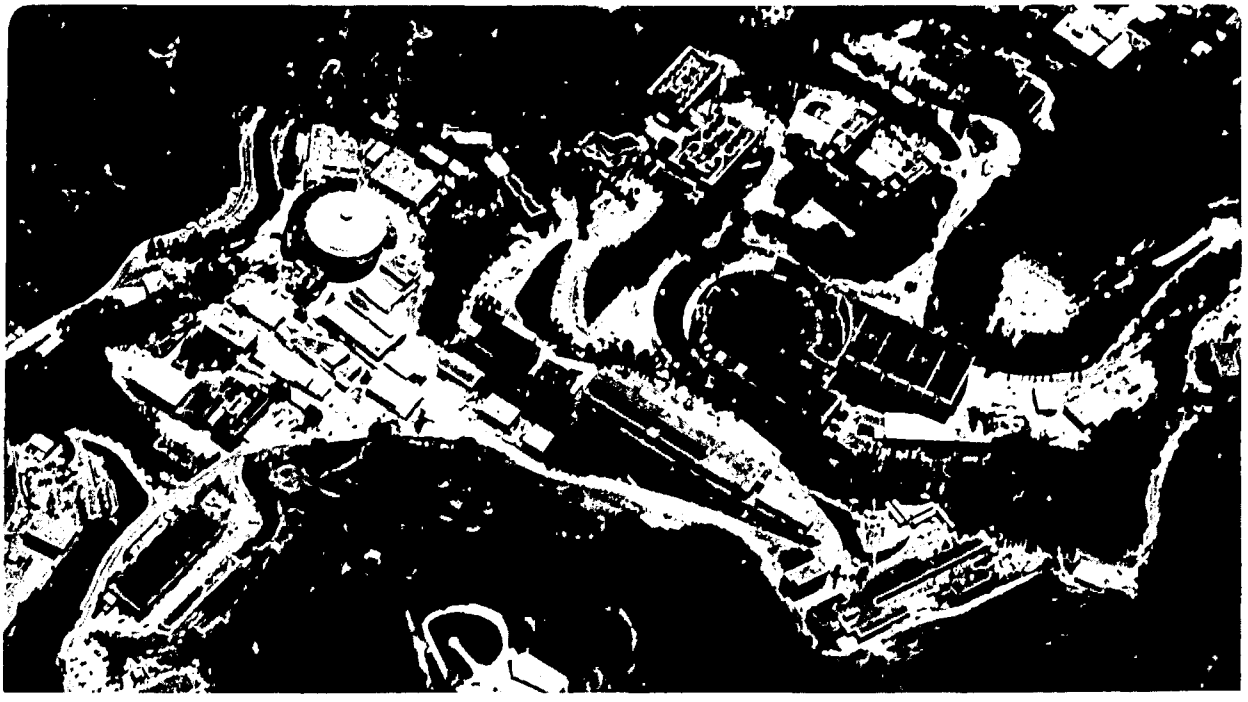

Prepared for the U.S. Department of Energy under Contract DE-AC03-76SF00098

DISCLAIMER

Development of a CCD Camera for an Automated Supernova Search
and Observations of a Supernova in NGC 5033

By

Michael Shane Burns

Lawrence Berkeley Laboratory
University of California
Berkeley, California 94720

Development of a CCD Camera for an Automated Supernova
Search and Observations of a Supernova in NGC 5033

ABSTRACT

Ph. D. Thesis

Michael Shane Burns
Lawrence Berkeley Laboratory
University of California
Berkeley, California 94720

The Berkeley supernova search uses an automated telescope along with a Charge Coupled Device (CCD) camera and a dedicated minicomputer to automatically scan galaxies for supernova. The system is currently able to observe about 500 galaxies in a full night of observing. These images are stored on video tapes which are brought back to the lab the next day for analysis. This paper begins with a brief summary of our theoretical understanding of supernova. The design of the search system is discussed with an emphasis on its current operation. The development and performance of the CCD camera is described in detail as well as the performance of the entire system. Finally, observations of a supernova in NGC 5033 are presented.

November, 1985

Acknowledgments

I would like to thank my thesis advisor, Rich Muller, for his guidance and for providing me with an example of how to do good science. Carl Pennypacker deserves special thanks for his constant encouragement and especially for trudging through the early drafts of this paper. Thanks to Frank Crawford not only for his help with the project but also for reminding me that physics is enjoyable. Jordin Kare and Saul Perlmutter helped with almost everything I have done and Roger Williams taught me most of what I know about computers. I would also like to thank James Graham for helping me better understand the physics of supernovae and for performing some of the data reduction on the supernova in NGC 5033. Finally I wish to thank Stormy for enduring the hardship of being married to a physics graduate student and my parents Bob and Connie Burns for both financial and moral support.

This work was supported by the Dept. of Energy under Contract No. DE-AC03-76SF00098.

Introduction

Supernovae are some of the most important and powerful events known to astrophysics. These cataclysmic explosions release as much as 10^{51} to 10^{53} ergs of energy over a period of one to two years and are probably responsible for acceleration of cosmic rays and the production and distribution of heavy elements. In addition, the interstellar shocks resulting from supernovae are likely to trigger new star formation. Neutron stars, pulsars, and black holes are almost certainly produced in supernova explosions. Besides being interesting in their own right, supernovae may also be useful for understanding the cosmological distance scale. Supernovae may be the best 'calibrated candles' in the universe. At maximum light, they are as bright as an entire galaxy.

Supernovae are extremely important to astrophysics, but they are not well understood. The reason for this lack of understanding is two-fold: the physics of the explosion is complex and there exist very few modern observations, especially before maximum luminosity. Several groups are making progress on the first of these problems with the help of sophisticated computer models (see for example Wilson et al. 1985; Hillebrandt et al. 1984). The reason so few modern observations have been made is that supernovae are rare by astronomical standards. Estimates for the rate range from one supernova per galaxy per 6 years (estimated from the pulsar birth rate) to one per galaxy per 600 years. Tammann (1982) has done one of the more detailed studies of supernova rates and has gotten an overall rate of roughly 1 per galaxy per 100 years. The low rate implies that a large number of galaxies must be searched frequently to 'catch' supernovae early in the explosion.

In 1978, inspired by Stirling Colgate's proposal for an automated supernova search, the LBL astrophysics group began work on a supernova search which uses an automated telescope in conjunction with an electronic detector, and a computer to observe large numbers of galaxies weekly and scan the images for supernova in real time. The Berkeley system uses a Charge Coupled Device (CCD) camera and a dedicated mini-computer (Digital Equipment Corporation PDP 11/44) for image analysis and telescope control. Much of the hardware and software is described in a Ph.D. thesis by Jordin Kare (1984).

The goal of the Berkeley group is to produce a system capable of searching about 6000 galaxies on a three night cycle and process the galaxy images in real time so that within a few seconds after the galaxy has been observed, a supernova candidate can be detected. Supernovae are found by comparing a newly acquired image with a previously acquired reference image. After some initial processing makes the images compatible, the reference image is subtracted from the new image. If a supernova is present, the difference image will show only the supernova.

Each night on the telescope (with good weather) about 300 images are observed and stored on video tape. The next day the tapes are brought back to the lab for processing. We have a data base of about 1000 reference images, which is scanned in about three nights of observing. With a supernova rate of 1 per galaxy per 100 years we expect to find about 10 supernova per year or about one a month.

1. Supernova

1.1. Supernova Properties

Although recent observations suggest several varieties of supernovae most are classified as Type I or Type II. Type I supernovae are distinguished from Type II by the absence of hydrogen lines, as well as by the presence of strong emission and absorption features in their spectrum. Figure 1.1 shows the spectrum of a Type I supernova observed at maximum light. The black body continuum is swamped by these strong features, whereas at maximum light the Type II spectrum is very close to a 10,000 °K black body. It is easy to see the Hydrogen lines in the spectrum of the Type II supernova 1983k (figure 1.2).

Type I and probably Type II supernovae increase their brightness from their pre-supernova level to their maximum luminosity in about two weeks, but Type I tend to be almost a full magnitude brighter on the average. The maximum B magnitude of Type I supernovae is $M_B = -19.7 + 5 \log(H_0 / 50$ km/sec/Mpc) with a dispersion of 0.4 magnitudes (H_0 is the Hubble constant). Type II supernovae have maximum luminosity of $M_B = -19.0 + 5 \log(H_0 / 50$ km/sec/Mpc) with a larger scatter of 1.6 magnitudes. If it is assumed that all Type I supernovae have the same maximum luminosity, then the uncertainty in the Type I magnitude is consistent with observational error and the uncertainty in the distance to the parent galaxy. Type IIs almost always occur in the dusty arms of spiral galaxies, so their brightness must be corrected for interstellar absorption. These corrections are difficult to make because of uncertainties in the amount of interstellar matter in the line of sight. However, even when these uncertainties are taken into account, the dispersion in the brightness of Type II supernovae is still large and likely to represent a real

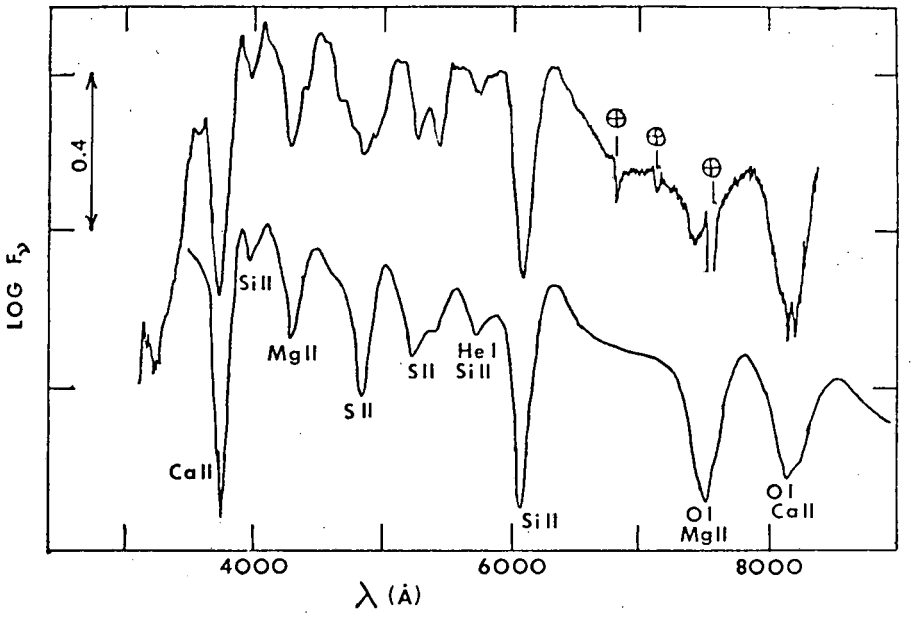

Figure 1.1 Spectrum of a Type I supernova near maximum luminosity. The top curve is the observed spectrum; the bottom curve is a synthetic spectrum created by Branch (1982).

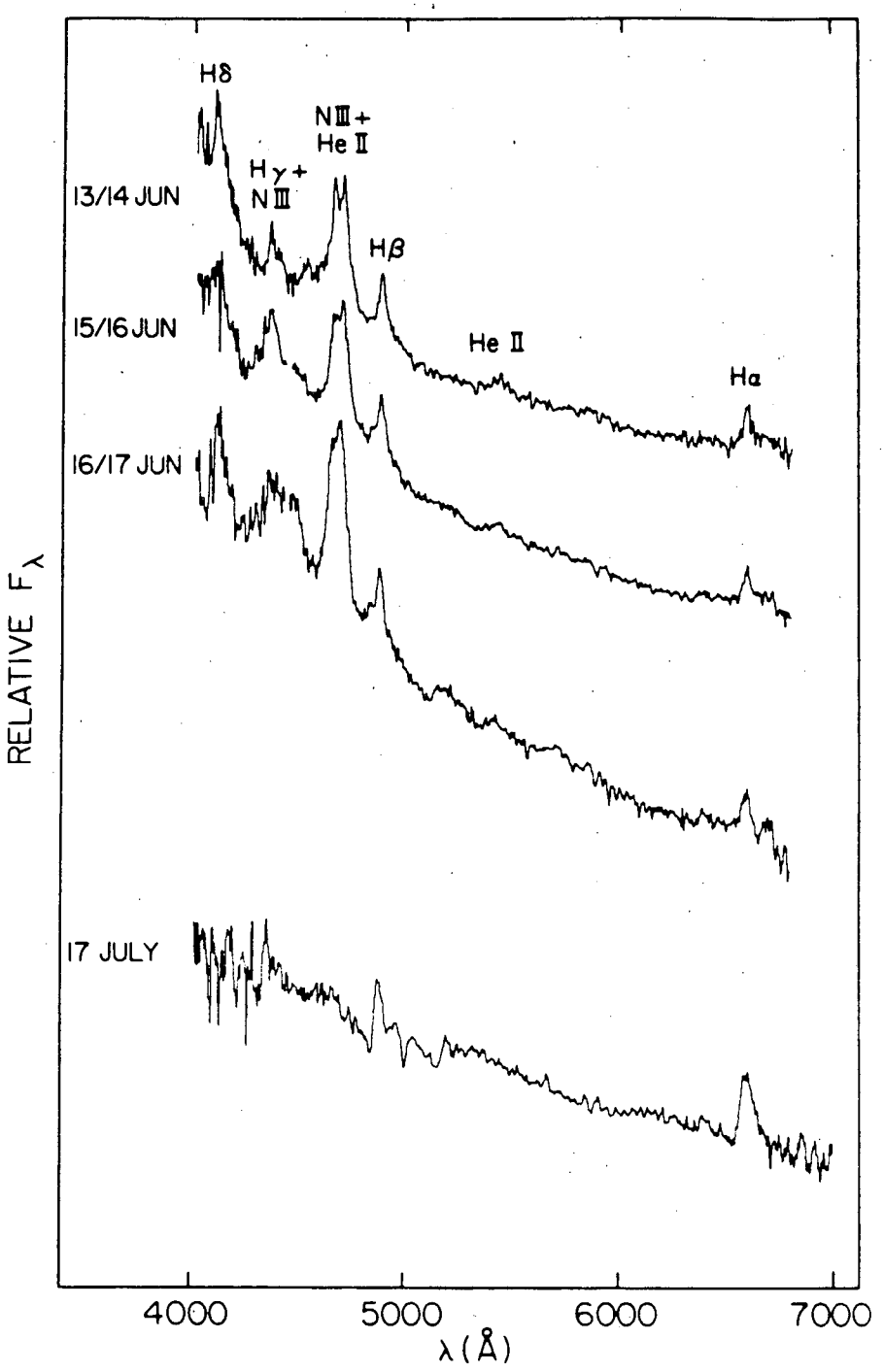

Figure 1.2 Spectrum of the Type II supernova 1983 k. (Niemla et al. 1985)

variation in their absolute magnitude. The high and consistent luminosity of Type I supernovae at maximum could make them the best standard candles in the universe.

The overriding observational parameter for developing a search strategy is the supernova event rate. Tammann (1982) has done one of the more systematic studies of supernova rates; his estimates are shown in Table 1.1. The rates are given in "supernova units" (SNu). One SNu is one supernova per 10^{10} solar luminosities per 100 years. His analysis implies a rate of about 1 supernova per galaxy per 50 to 100 years for a typical galaxy. Note that Type II supernovae have never been observed in elliptical galaxies. Furthermore, there is evidence that Type II supernovae occur almost exclusively in the arms of spiral galaxies. However, galactic cores are undersampled since most supernovae have been discovered using photographic plates in which the core is saturated. By using a charge coupled device (CCD) with its large dynamic range, the Berkeley search should be able to see supernovae in galactic cores and hence understand better how these events are distributed within a galaxy.

	All SN	Type I	Type II
E	0.22	0.22	0.0
SO	0.12	0.12	0.0
SOa, Sa	0.28	0.28	0.0
Sab, Sb	0.69	0.37	0.32
Sbc, Sc, Scd, Sd	1.38	0.77	0.61
Sdm, Sm, Im	1.02	0.83	0.19
IO			undetermined

Table 1.1 supernova frequencies in SNu for different types of galaxies (Tammann 1982).

1.2. Supernova Models

1.2.1. Type I Models

Currently, the most successful Type I model hypothesizes a carbon-oxygen (C-O) white dwarf accreting mass from a companion (Iben and Tutukov 1984). The accreted hydrogen quickly burns to helium which ignites and burns to carbon at the surface of the dwarf's core. As the Chandrasekhar mass is approached, the carbon ignites and a detonation or deflagration wave propagates through both the core and the mantle converting a large fraction of the dwarf's mass into ^{56}Ni.

The ^{56}Ni decays to ^{56}Co with a half-life of 6.1 days which in turn decays to ^{56}Fe with a half-life of 77 days. The decay of this Ni is thought to power the declining part of the light curve (Colgate and McKee 1969). The luminosity of Type I supernovae drops two to three magnitudes below maximum in the first 30 days. The half-life of the steepest part of the light curve is 5-10 days which is close to the half-life for the decay of ^{56}Ni to ^{56}Co. Colgate and McKee (1969) developed a model in which the early part of the light curve is powered by the thermalization of the gamma rays and positrons emitted in the decay of ^{56}Ni. The more slowly decaying portion of the light curve has a half-life of 50-60 days and is thought to be powered by the decay of ^{56}Co to ^{56}Fe. Axelrod (1980) has been successful in using this model to explain the observed light curve and late time spectrum of Type I supernovae. Recently, Graham, Meikle, Allen, Longmore and Williams (1985) observed strong Fe II line emission at 1.664 μm in supernova 1983n which strongly supports the scenario outlined above. They were able to estimate from their observations that 0.3 solar masses of iron were present.

1.2.2. Type II Models

The most likely model for Type II supernovae is a variant of the theory developed in the paper by Burbidge, Burbidge, Fowler, and Hoyle (1957). A new star starts its life as a cloud of hydrogen which collapses and heats until the temperature and pressure inside are sufficient to ignite the core hydrogen and burn it to helium. The energy generated balances the gravitational contraction until the core hydrogen is used up. The core then contracts further until its temperatures and densities are high enough to ignite the core helium. Through this process the star burns progressively heavier elements in its core, and if it is massive enough, develops the onion skin structure shown in figure 1.3. Stars with mass less than the Chandrasekhar mass (~1.4 solar masses) end their lives as white dwarves when the burning stops with a carbon oxygen core supported by electron degeneracy. A star more massive than about ten solar masses can undergo nuclear transformation until the core contains 1.5 solar masses of iron. The binding energy per nucleon is a maximum for iron so no more energy can be extracted from the core by fusion. Type II supernovae are thought to occur when the mass of the iron core exceeds the Chandrasekhar mass and can no longer be supported by electron degeneracy pressure. The core begins to collapse and heat until thermal photons begin to break up the iron nuclei (photodisintegration) which robs energy from the core, leading to further collapse. Photodisintegration also makes protons available for electron capture which reduces the number of electrons, lowering the electron degeneracy pressure. As the collapse continues, the density in the center of the core begins to approach the density of nuclear matter and the pressure begins to build. The core is

compressed beyond nuclear density and then rebounds sending a pressure wave out through the in-falling matter. The pressure wave steepens into a shock wave at 0.7 to 0.8 solar masses from the center and then propagates out toward the star's mantle. What happens to the shock next has been the subject of much debate and depends on the strength of the shock, the neutrino opacity of the core, and the neutrino opacity and structure of the mantle.

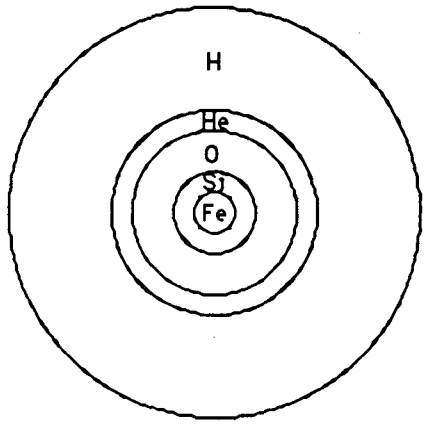

Figure 1.3 "Onionskin" structure of a Type II supernova progenitor star (adapted from Trimble 1982).

One of the biggest uncertainties in all calculations of supernova properties is the nuclear equation of state at the extreme temperatures ($\sim 10^{10}$ °K) and densities ($\sim 10^{9}$ gm/cm^3) in the collapsing iron core. It is difficult experimentally to determine the equation of state from nuclear scattering experiments, so calculation must be relied upon. One problem with early supernova models was that although the collapse occurred and produced a shock, it didn't have enough energy to cause a supernova explosion. Recently, new techniques have been used to calculate the

equations of state with the result that the core compressibility is 2.5 times what had been assumed in the past (Bethe, Brown, Cooperstein, and Wilson 1983). The larger compressibility means that the core can be more strongly compressed so that the rebound is energetic enough to push the shock out through the mantle of the star and produce a supernova which releases about 10^{49} ergs of electromagnetic radiation. This mechanism, by itself, can only generate supernovae from progenitor stars whose mass is in the range of between 12 and 18 solar masses.

Recently, Wilson, Mayle, Woosley, and Weaver (1985) have used computer models which include the effects of neutrino heating to produce supernovae from stars as massive as 50 solar masses. When first running these core collapse simulations, it was found that about 0.5 seconds after collapse, the shock began to weaken and stall as its energy went into photodisintegration of iron. However, about 0.7 seconds after collapse the shock regenerated and produced a supernova. The shock was reheated by the neutrinos released during electron capture. At densities in the core greater than 10^{11} gm/cm^3, the neutrinos are trapped. The hot neutrinos diffuse out of the core, however, and interact strongly enough with the relatively cool shock to reheat and revive it. Figure 1.4 shows the mass-radius contours plotted against time after core bounce for a 25 solar mass progenitor with an iron core of 1.63 solar masses (the radius of the shock is the heavy black line) (Wilson et al 1985). At 0.55 seconds after core collapse, the shock has stalled and has even begun to recede, but by 0.7 seconds it has regenerated and by .75 seconds is well on its way to blowing off the star's mantle. The explosion energy for this model is 1.1×10^{51} ergs and the neutron star remnant mass is 1.58 solar masses.

So far, models for supernovae from progenitor stars of 11 solar mass and higher have been discussed. Yet the supernova that produced the Crab nebula and pulsar is estimated to have been created by the explosion of a star with a main sequence mass of no more than 10 solar masses (Nomoto 1982). It is thought that stars in the mass range of about 8 to 11 solar masses do not reach the temperatures and densities in the core required to produce iron. These stars begin to collapse when a core of oxygen, neon, and magnesium reaches the Chandrasekhar limit. As in the iron core models, a shock is produced when matter rebounds off a nuclear degenerate core. However, the shock loses less energy to photodisintegration because the binding energy of carbon and oxygen is smaller than that of iron. In addition, the mantle of these relatively light stars is less massive so less energy is required to blow it off. Hillebrandt, Nomoto, and Wolf (1984) have investigated this model with computer simulations and have gotten supernova explosions with total energies of 2×10^{51} ergs. Nomoto suggests that the Crab pulsar and nebula were the result of just such a supernova.

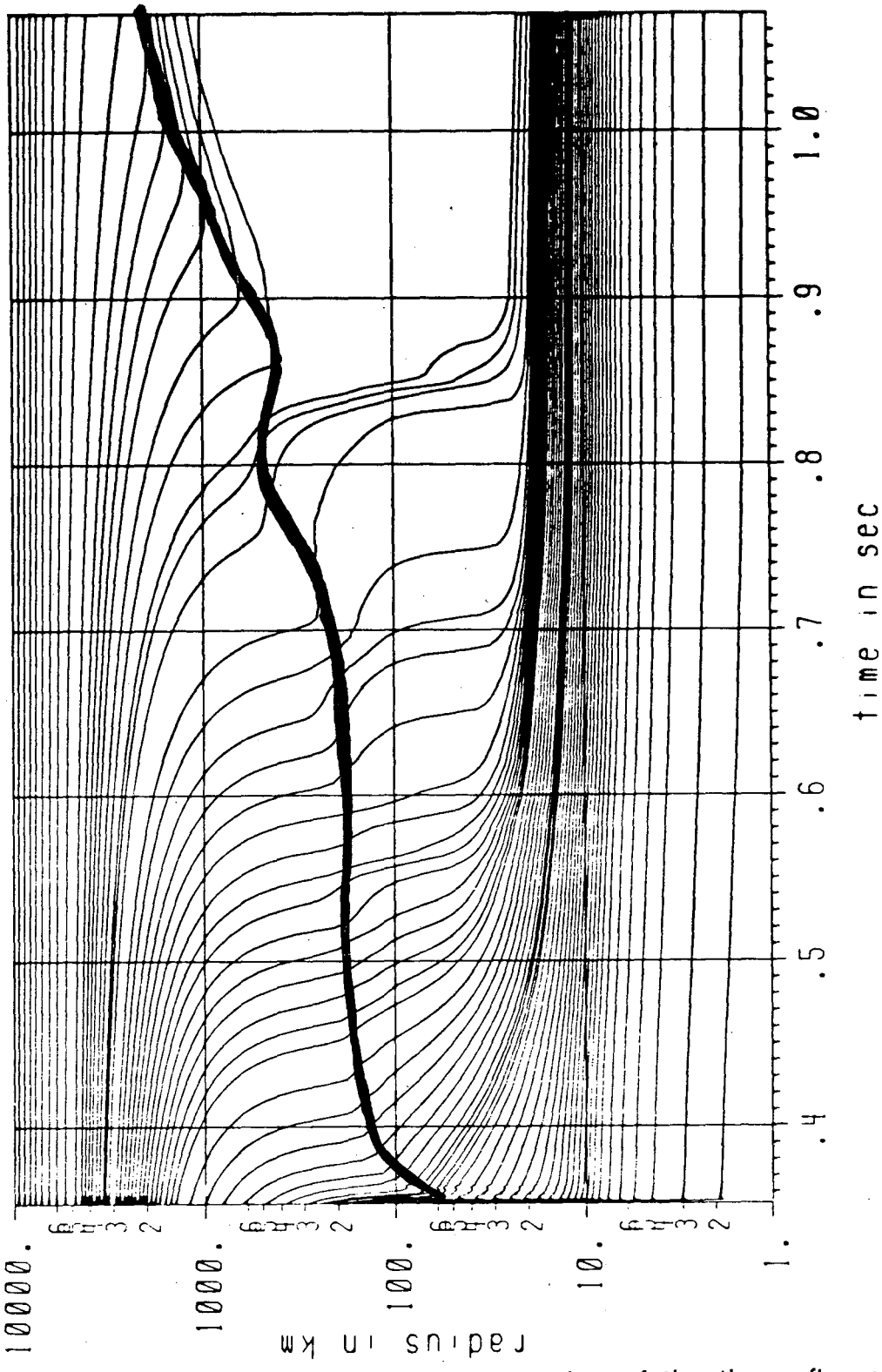

Figure 1.4 Mass-radius contours as a function of the time after core collapse. The heavy black line shows the radius of the shock (Wilson et al. 1985).

2. Current Design of the Berkeley SN Search

2.1. Overview

One of the main goals of the supernova search is to image 6000 galaxies each week and process these images in real time. (For a description of the design goal see Kare et al. 1982.) This is to be accomplished by using a CCD camera and a small automated telescope. The telescope moves from one galaxy to the next and exposes the CCD automatically while the last image is analyzed. Currently, the system is able to acquire galaxy images automatically at a rate of about 600 per night and record these images on video tape. The tapes are taken to the lab in Berkeley the next day where they are read into the image analysis computer. The images are processed and a list of SN candidates is generated automatically. The next two sections describe the observation and image analysis systems that are currently in use.

2.2. Observation System

Figure 2.1 is a block diagram of the observing and image analysis systems. The telescope is the 30 inch Ritchey-Chretien (f/8) reflector at the Leuschner Observatory which is 12 miles east of the Berkeley campus (for a complete description of the observatory see Treffers 1984). When we began using this telescope in the spring of 1984, it was already controlled by a PET micro-computer which has since been upgraded to an IBM Personal Computer (PC). Programs for the PC were written in compiled BASIC to allow the telescope control computer to accept information from our PDP 11/44 in Berkeley. During observations, the 11/44

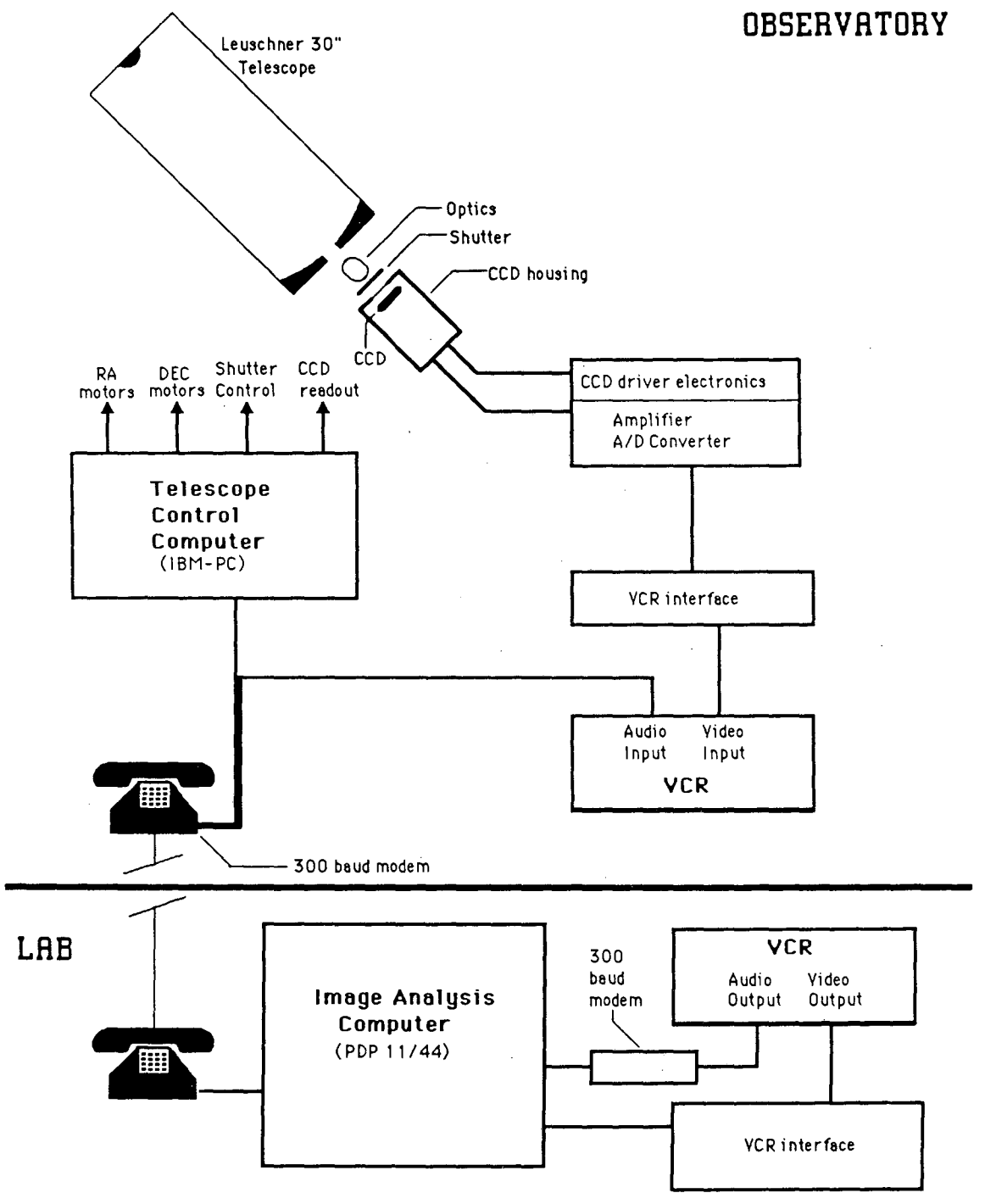

Figure 2.1 Block diagram of the supernova search system.

sends the coordinates, exposure time, and object name over a phone line to the IBM PC. The PC points the telescope, opens the shutter, sends a signal to the CCD electronics to start a CCD read-out, then notifies the 11/44 that the first cycle is complete. This cycle is repeated automatically 25 to 100 times depending on the size of the observation list. The observer then checks the telescope by pointing on a bright star and begins another observation list. All of the communication between the two computers is done via 300 baud modems. The modem signal is recorded on the audio track of the video tapes used to record the CCD data. During image processing, the audio signal is monitored by the image analysis computer (the PDP 11/44) and used to keep track of which galaxies are being analyzed.

The CCD camera consists of an RCA CCD (model # SID 53612XO) mounted inside an aluminum vacuum housing so it may be cooled to reduce thermal noise. A preamplifier inside the housing (but not cold) amplifies the signal which is then fed to another set of amplifiers and an analog to digital converter (ADC). The ADC and final stage of amplifiers are contained in an electronics package along with the CCD driver electronics. This package is mounted on the telescope separately from the vacuum housing.

The CCD being used is an array of 512 by 320 photosensitive cells or pixels; each pixel is 30 μm square. The plate scale for a 30 inch f/8 telescope is 0.56 arc-minutes/mm, so for the Leuschner 30 inch telescope each pixel would cover a patch of sky 1.0 arc-second on a side. The seeing at the Leuschner site is typically 3 to 4 arc-seconds so a SN image would be spread over several pixels. For the 30 second exposures used in the search, the pixel read out noise dominates over sky

background noise (§ 4.1.1) so spreading the SN signal over several pixels reduces the signal-to-noise ratio and thereby our detection limit. In order to reduce this problem, a Nikon lens is used to reduce the image to a plate scale of 1.34 arc-minutes/mm. Each pixel then covers a square of sky 2.4 arc-seconds on a side. The shutter (Uniblitz model #225LOAOX5) sits just behind reduction optics and is opened and closed on signals from the telescope control computer.

The serial digital signal from the electronics package is transferred through fiber optics cables to a video cassette recorder (VCR) interface. This interface converts the serial signal into a form that can be stored easily on video tape. The output of this interface is connected to the input of a slightly modified Sony Betamax VCR and is stored on video tape. (For a complete description of this video interface see Kare 1984).

2.3. Image Analysis

2.3.1 Overview

After the tapes are brought back to the lab, they are played back on another VCR. The video signal is sent to an interface which converts the video signal back into a digital serial signal identical to the one from the CCD. The serial signal is fed into a first-in first-out buffer where it is stored until the 11/44 is ready to transfer the signal directly to memory. The audio track is translated by a 300 baud modem and goes to another port on the computer. The audio track information is received by the image analysis program and used to keep track of what is on tape. The program which transfers information from the video tape to memory can read and process an

entire video tape automatically. Its modular design separates data acquisition from image processing so that the same "shell" program can be used for reference image building, searching for SN, or any other image analysis we choose to perform.

2.3.2 Reference Image Analysis

The first step in creating a reference image is to correct the raw image for quantum efficiency variations across the CCD, image vignetting by the reduction optics and the dark frame bias. This is done by subtracting a dark frame from the raw image, then multiplying the result by a system efficiency frame. The dark frame is generated by calculating the median of three unexposed CCD frames taken at the telescope. Using a median of three frames eliminates tape dropouts (which are set to zero by the video interface) and bright pixels which may have been generated by cosmic rays passing through the CCD. The dark frames have an arbitrarily set average count per pixel of about 430. A typical dark frame is shown in figure 2.2. The system efficiency frame is generated from three exposures of the sky taken at dusk or dawn on each night's observing. The median dark frame is subtracted from each sky frame and then inverted. These inverted sky frames are then normalized to an average count of 1000 to produce a system efficiency frame. A median of these three efficiency frames is taken to eliminate tape dropouts and stars which may have appeared in an individual sky frame. Figure 2.3 shows a typical median system efficiency frame produced by the procedure outlined above. After being multiplied by the median system efficiency the raw reference image is divided by 1000.

The reference image builder subroutine's main functions are to generate a

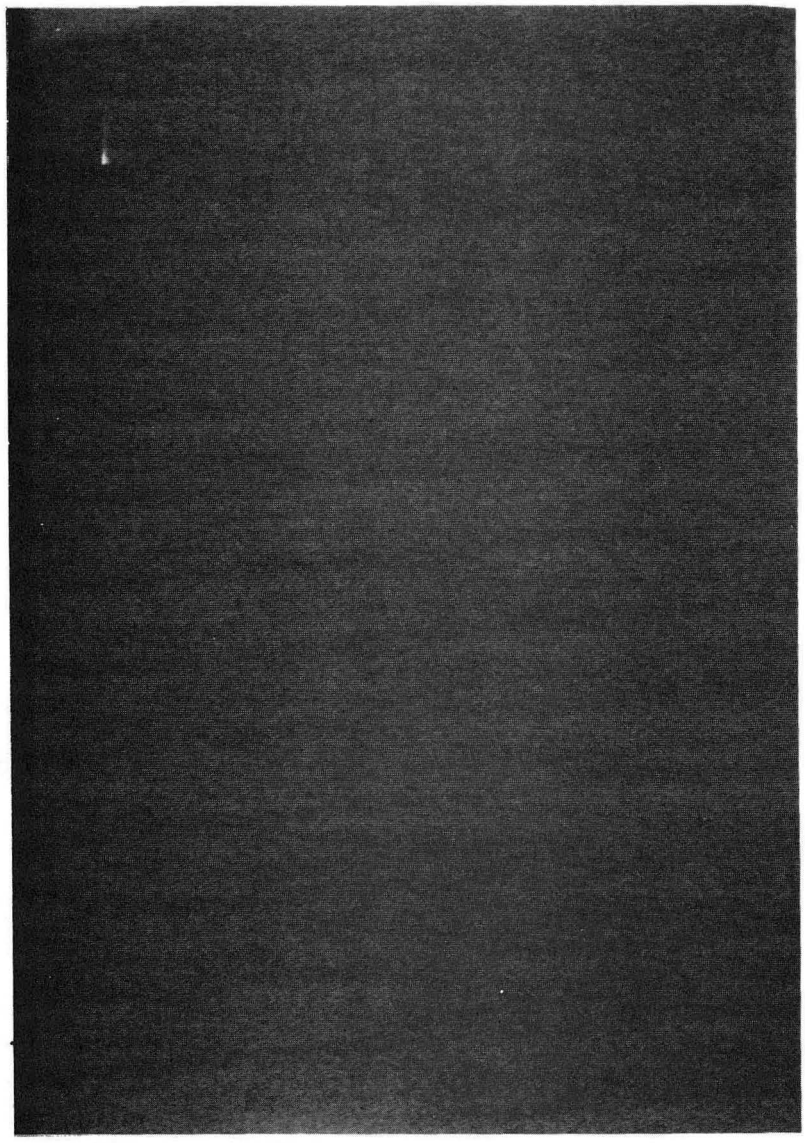

XBB 861-452

Figure 2.2 Typical dark frame.

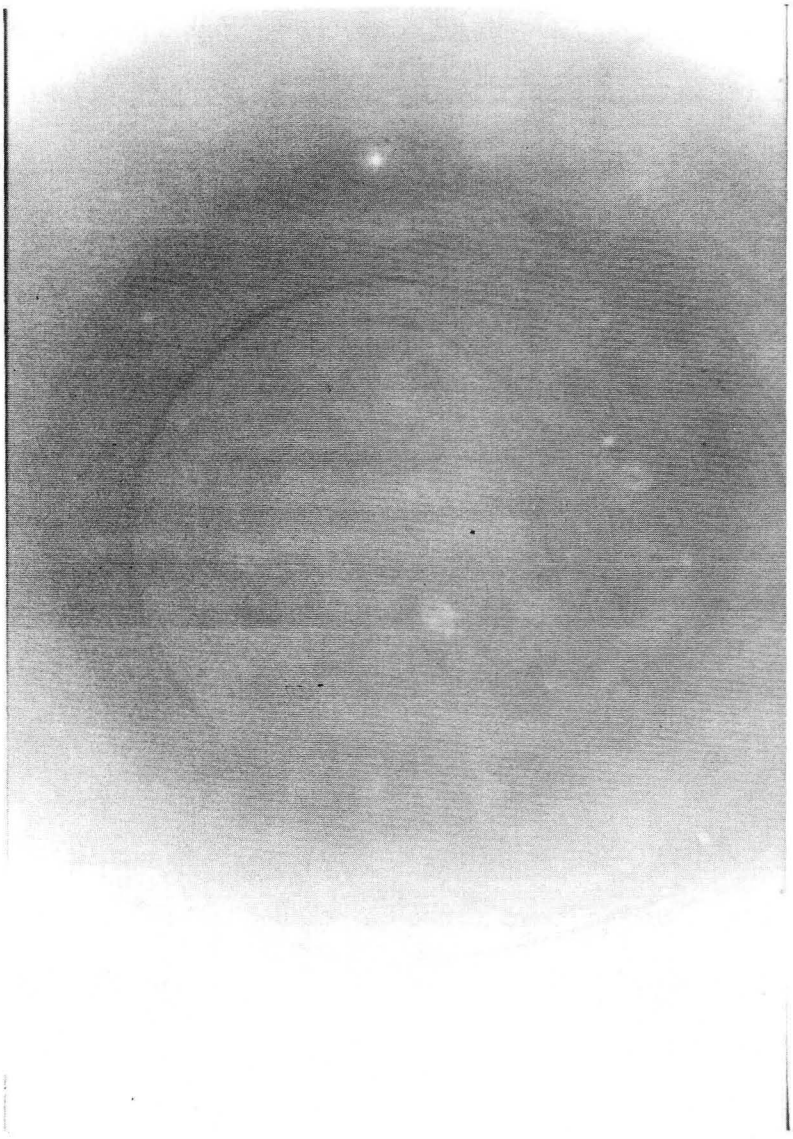

XBB 861-453

Figure 2.3 Typical system efficiency frame.

subimage of the galaxy, store that image in the reference subimage array (.RSA) disc file, store information about the galaxy in the reference subimage parameters (.RSP) file, find several fiducial stars, and store their positions and brightness in the object catalog (.OBC) file. In addition to these primary functions, the routine also logs the date these files were created in a chronological log file (.CLG). If the program runs successfully, the galaxy's name is found in one of the galaxy sky block files and marked as an object to be put on a supernova search list. Each sky block file has a list of all the galaxies in a block of sky one hour of right ascension wide by 10° of declination long. For a more detailed description of these files see Appendix I.

For each galaxy, all of the files generated by the reference builder subroutine have the same name except for the extension. The name is a concatenation of the sky block file name, a character to specify which galaxy in the reference image these files are for, and the number of the galaxy in the sky block file. For example, the name 'B15P4B002' is created from the sky block name B15P4, B (which identifies this galaxy as the second one found in the reference image), and 002 (which identifies the galaxy as the second one listed in the sky block file B15P4). The sky block names are described in Appendix I.

Figure 2.4 is an outline of the reference builder subroutine. The subroutine starts by reading a start-up file that contains information used later in the program. Included in this file are the name of the device and directory in which the output files are to be stored. The subroutine can run in a manual as well as an automated mode;

Automated Reference Builder

Inputs: Sky Block File Name, Galaxy Number, Date of observation

Outputs: Error Flag

Read Start-up File

(Start-up file contains: device and directory of created files, expected coordinates of galaxy, mask file name, and manual operation flag.)

Mask edges and "bad" sections of CCD

(Bad pixels are set to zero.)

Generate fiducial star list

-Find approximate positions of starts

-Calculate centroid for each star (1/3 pixel accuracy)

-Write fiducial star coordinates and brightness to the object catalog file (.OBC)

Find galaxy

-Generate list of galaxy candidates

-Choose among candidates

(If no galaxy is found and running in automated mode, the name of the galaxy is written to the file 'nogalaxy.lis'.)

Display "cleaned" image and run joystick (only if using manual mode)

Request user to verify galaxy coordinates (only if using manual mode)

Write galaxy framing, coordinates, and exposure time to the reference subimage parameters (.RSP) file

Transfer galaxy image from memory to disc file (.RSA)

Flag galaxy as built and write date of observation to galaxy list files.

END

Figure 2.4 Outline of reference image builder program.

a flag is read from the start-up file to set the program to automated or manual mode.

The first step in reference image processing is to mask CCD defects and the edges of the image. The vignetting along edges of the CCD is so severe (up to 90% of the light is lost in one corner) that the system efficiency correction cannot compensate for it well enough to be able to use the stars along the edges as fiducials. Another problem feature is a "flare" defect in the upper left hand corner of the CCD (see figure 2.2). This flare looks like a star to the image analysis software so it is masked. Masking consists of setting all the masked pixels to zero. The rest of the image analysis software is designed to ignore zero value pixels.

The next step in the processing is to find the fiducial stars. These are stars used to align the reference image with the search image, and estimate sky transmission during the search phase of the image analysis. The stars are found by searching the entire image for bright groups of pixels. A centroid in a 16 by 16 pixel patch around each group is calculated to find the star's position to within about 1/3 of a pixel. The coordinates of each star as well as its integrated brightness is written to the .OBC file.

An entire CCD frame takes up about 1/3 of a megabyte of memory, so storing the entire reference image on disc is impractical. To reduce the amount of disc space required, we store only a 100 to 200 pixels square region around the galaxy's core. The first method used to find galaxies was to have someone look at a display of the cleaned image and type its coordinates into the computer. After looking at a hundred or so images it became apparent that on any given night the galaxies in successive

CCD frames would appear within about 30 pixels of each other. We also discovered that the galaxies have a larger full width at half maximum than stars by a factor of about 2 to 4. We now use a subroutine called by the reference builder to search the region where the galaxy is expected to appear and then generate a list of galaxy candidates. Another subroutine then chooses among the candidates by scoring each object by how close it is to its expected position and its full width at half maximum. If no good candidate is found and if the program is being run automatically, the name of the expected galaxy is written to a file so that it can be looked at manually.

If the program is being run manually, the cleaned image is displayed on the Grinnell system and the user is asked to verify the galaxy coordinates (or the expected galaxy coordinates if no galaxy was found automatically). The expected coordinates are calculated by keeping a running average of the coordinates of found galaxies. Once the galaxy center is found, a 150 by 150 pixel block around the galaxy is transferred to the .RSA disc file. The last step in the image building process is to flag the galaxy as built and write the date of observation into the sky block files.

2.3.3 Search Image Analysis

The subroutine used to process the searched images is called from the automated shell program in much the same way as the reference image building program is called, except that the new search image is not corrected for system efficiency. There is no reason to correct the entire image, since only the subimage containing the galaxy and patches around the fiducial stars are used in the processing. The processing starts by first finding the stars in the new image and

comparing the positions of these stars with the positions of the reference fiducial stars recorded in the .OBC file. After the current image stars are matched with the reference stars, the brightness of each set of stars is used to calculate a scaling factor by which the new image is multiplied. This takes care of any change in sky transmission from night to night. Once an offset is found between the reference image and the new search image, the new subimage containing the galaxy is scaled, cleaned, and then stored in memory. The next step is to retrieve the reference image from disc and store it in memory. The reference image is shifted by a fraction of a pixel to match the new image, then subtracted from the search image. The resulting difference image is stored on disc with the file extension .DIS. We are currently storing the difference image to make it easy to test different supernova finding algorithms. After a dependable algorithm is decided upon, the difference image will be scanned for SN instead of being stored. The simplest finding algorithm starts by calculating the rms variation from pixel to pixel (σ) in the difference image and then searches the image for all pixels 5σ above the average background level. This algorithm by itself will also find statistical fluctuations, cosmic rays that generate charge in the CCD, and asteroids that happen to be in the field of view during the exposure. All of these false alarms can be eliminated by observing the field again the next night or when analyzing the images in real time, observing the field again an hour later the same night (a typical asteroid moves about 30 arc-seconds in an hour).

Another class of false alarms occur because of slight misalignments of the reference with search image or improper corrections for atmospheric seeing. When these problems occur, some pixels in the search image are over-subtracted while nearby pixels are under-subtracted. Figure 2.5 shows a difference image generated

by the automatic subtraction routine. There are only two regions in the difference image that have pixels with values greater than 5σ above the background. One of these regions is centered on the galaxy core and the other is associated with the foreground star in the lower right-hand corner of the difference image. Figure 2.6 shows the pixel values in these two regions. The background level is 677 ADU and $\sigma = 3.8$. There is one pixel in each of these images that is more than 5σ above the background: one in the galaxy image at row 53 and column 52, and the other in row 12 and column 96. These false alarms can be eliminated by calculating the average of the 3 by 3 block centered on the candidate pixel. If the candidate results from misalignment or improper seeing corrections, then the over-subtracted pixels will compensate for the under-subtracted pixels and the average will be near the background level. If the candidate is a supernova, the 3 by 3 average will be higher than the background. A threshold for detection can be set by examining a large number of difference images and adjusting the threshold to give an acceptable false alarm rate.

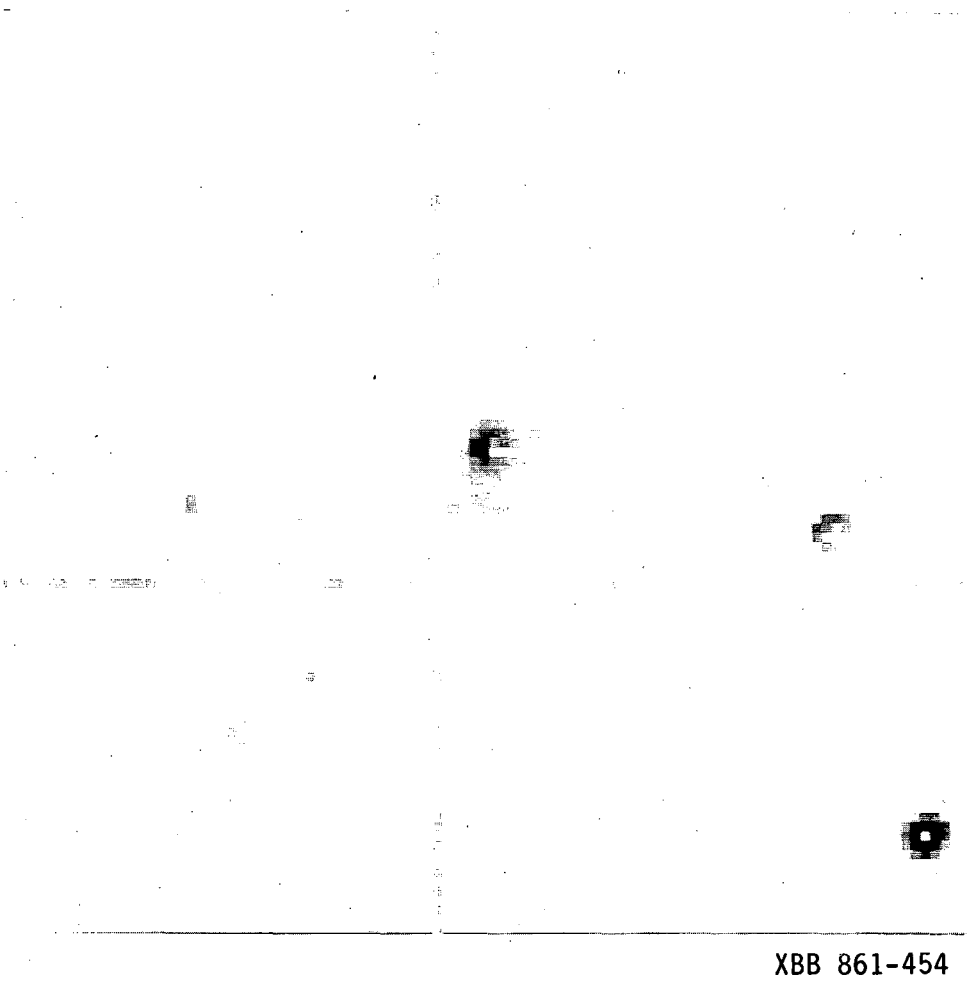

Figure 2.5 A difference image of NGC 6207 produced by the automatic subtraction routine.

	47	48	49	50	51	52	53	54	55	56
49:	666	660	658	664	657	659	667	673	670	667
50:	671	662	667	654	662	659	668	666	665	679
51:	669	667	659	651	645	647	659	671	668	670
52:	662	660	658	643	622	644	651	660	663	674
53:	672	667	655	608	619	715	660	668	667	662
54:	668	666	659	619	601	654	638	655	671	669
55:	665	666	664	648	625	631	645	664	666	659
56:	678	669	667	660	649	657	661	673	671	671
57:	672	679	668	666	668	663	664	667	666	668
58:	667	669	671	665	667	664	667	664	674	672

(a)

	91	92	93	94	95	96	97	98	99	100
8:	675	671	678	677	675	668	675	676	677	674
9:	677	681	671	676	672	674	672	676	682	679
10:	683	679	677	667	640	621	645	670	673	675
11:	678	675	676	648	592	605	587	658	678	677
12:	676	675	672	637	575	811	544	632	681	675
13:	681	670	676	648	591	579	533	632	676	678
14:	674	671	680	668	658	638	641	666	674	676
15:	672	673	672	674	675	670	672	669	675	676
16:	680	673	672	678	678	671	674	671	671	671

(b)

Figure 2.6 Printout of the pixel values in the difference image around the galaxy core (a) and around a foreground star (b).

3. Development of the CCD Camera

3.1 Introduction

A CCD camera is well suited to a supernova search. The supernova search requires an imaging detector whose output can be digitized quickly so the galaxy image can be processed in real time. A detector with low noise and high quantum efficiency must be used to minimize the exposure time for each galaxy. A large dynamic range is required so the cores of galaxies will not saturate the detector. The RCA CCD being used in the SN search has an rms noise of 86 ± 15 electrons per pixel and can hold 500,000 photoelectrons before saturating. The manufacturer's quantum efficiency curve is shown in figure 3.1, but the measured efficiency of our chip at a single wavelength was lower by a factor of two (see section 3.3.4).

To understand how a CCD stores charge, consider figure 3.2 (a) which shows a single unit of a CCD array. A silicon oxide layer insulates the p-type material from the electrode. If a positive potential is placed on the electrode, the holes in the substrate will be driven away from the electrode, forming a hole depleted region. If an electron is excited to the conduction band in this depletion region (by an incident photon for example), it will be collected in a thin layer just below the electrode. The hole will migrate away from the electrode, effectively storing the electron under the electrode. This type of device is called a surface channel CCD because the electrons are stored very close to the semiconductor insulator interface. The charge transfer efficiency of these devices is limited by states near the surface of the semiconductor, which are the first to acquire charge but are reluctant to give it up when the charge is to be transferred to the next pixel. This problem is reduced by putting an n-type

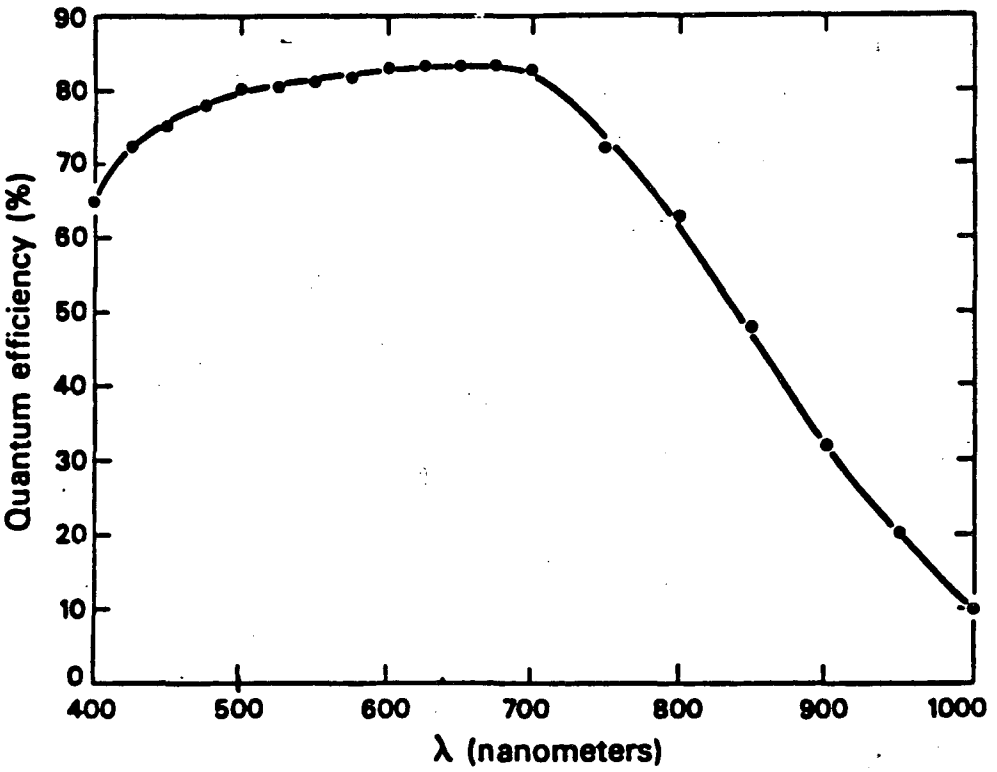

Figure 3.1 Manufacturer's quantum efficiency curve for the RCA backside illuminated CCD.

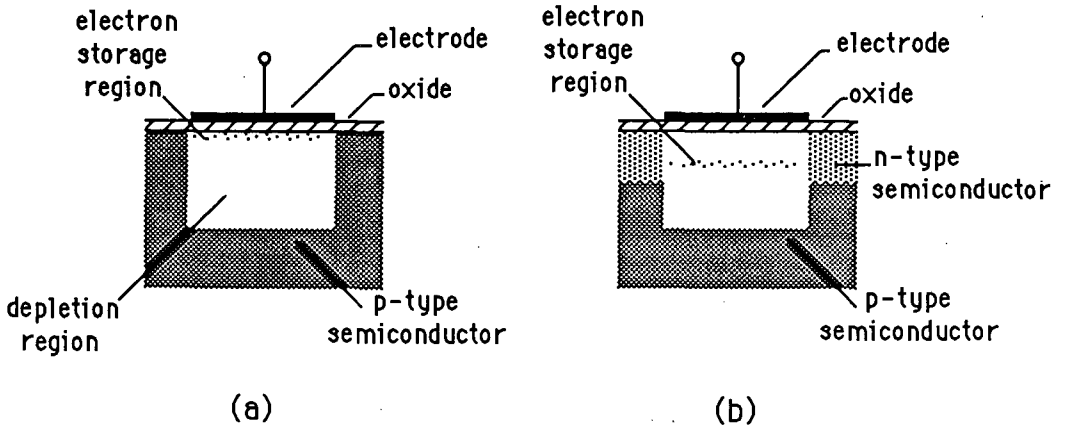

Figure 3.2 Single CCD electrodes for a surface channel CCD (a), and a buried channel CCD (b).

material between the substrate and the oxide layer (figure 3.2 (b)). In these buried channel CCDs the charge is stored at the pn junction rather than near the surface. Surface trapping does not occur in buried channel devices, so the charge transfers more efficiently.

Charge is moved along the CCD by using three electrodes for each pixel (three phase CCD). Figure 3.3 shows a portion of a linear CCD array as the charge is moved from one pixel to another. In figure 3.3 (a), photoelectrons are stored under the second set of electrodes which is held positive. Electrode sets one and three are held negative. The charge packets are moved to electrode set three by raising the potential of set three, then lowering the potential of set two (figures 3.3 (b) and 3.3 (c)). The process is repeated with electrode sets three and one, then with one and two at which point the charge has been moved from pixel A to pixel B. The electrode arrangement for a two dimensional CCD is more complex. Three electrodes cover each row of pixels. The columns of pixels are separated by a channel stop diffusion between each pixel. The CCD is read out by first shifting the contents of each row down by one row. The bottom row of charge is transferred to the horizontal readout register. This register then transfers the charge packets one by one to the output amplifier. After the horizontal register is empty, another vertical transfer fills it and the horizontal register is read out again.

The CCD currently being used for the SN search is an RCA model SID53612XO buried channel, three phase device. The substrate on this model is supposed to be thinned to less than 10 μm . Thinning allows it to be illuminated from the side opposite the electrodes which improves the device's quantum efficiency. The CCD

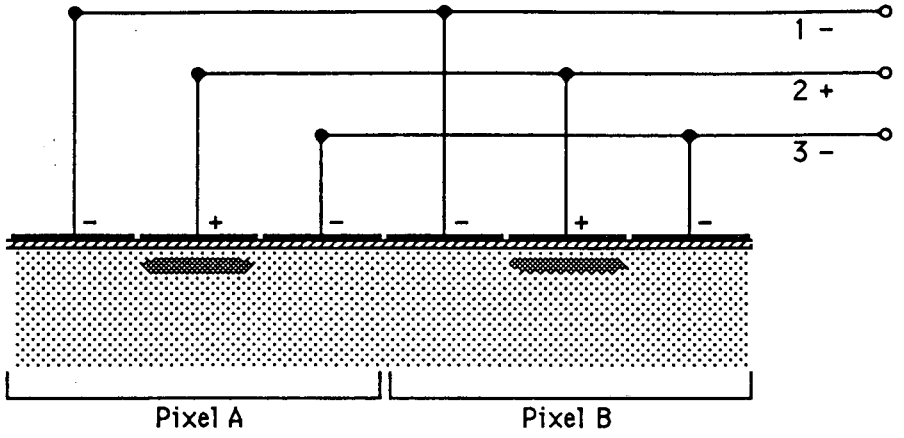

(a)

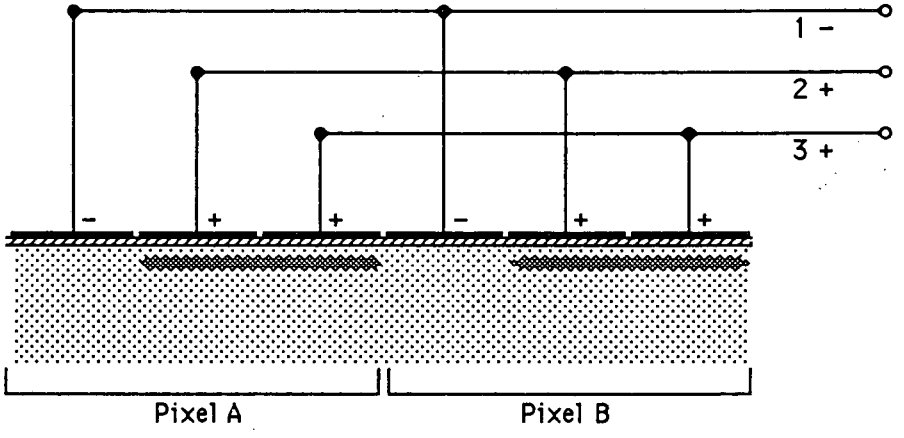

(b)

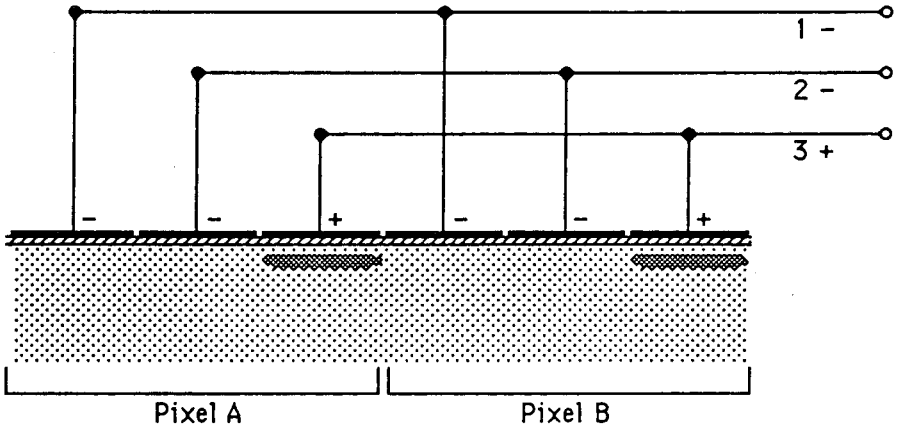

(c)

Figure 3.3 Movement of a charge packed during transfer.

was loaned to us by RCA pending delivery of a higher performance model SID501DX which was recently delivered and is currently being tested. The new device is supposed to have better charge transfer characteristics and lower noise (40 instead 90 electrons per pixel rms).

3.2 CCD Electronics Design

3.2.1 CCD Driver Electronics

A total of seven clocked signals are required to readout the CCD: three phases for the horizontal register, three for the vertical registers and a reset clock to reset the CCD output gate before the next charge transfer. Figure 3.4 shows the phases and typical voltages of these clocks. Each horizontal and vertical clock pulse is 2.5 μs wide and overlaps the neighboring pulse by 2 μs. The reset pulse is 2 μs wide and has the same period as the horizontal register clocks (50 μs). After 320 horizontal transfers, one horizontal transfer is skipped while a vertical transfer takes place to refill the horizontal register. The phasing of the three vertical clocks is the same as the horizontal clocks but the period is 16 ms (320 × 50 μs) so it takes about 8.2 seconds to read the entire CCD.

The electronics which generate these clocks are based on a design by John Geary of the Harvard Smithsonian Observatory. The schematics and a detailed explanation of the circuits are in a senior honors thesis by John Culver (1982). The digital electronics which generate the timing is controlled by a 2 Mhz crystal. (The CCD can be read out in 4 seconds by replacing the 2 Mhz crystal with a 4 Mhz crystal. This must be done to reach the design goal of searching 2500 galaxies per

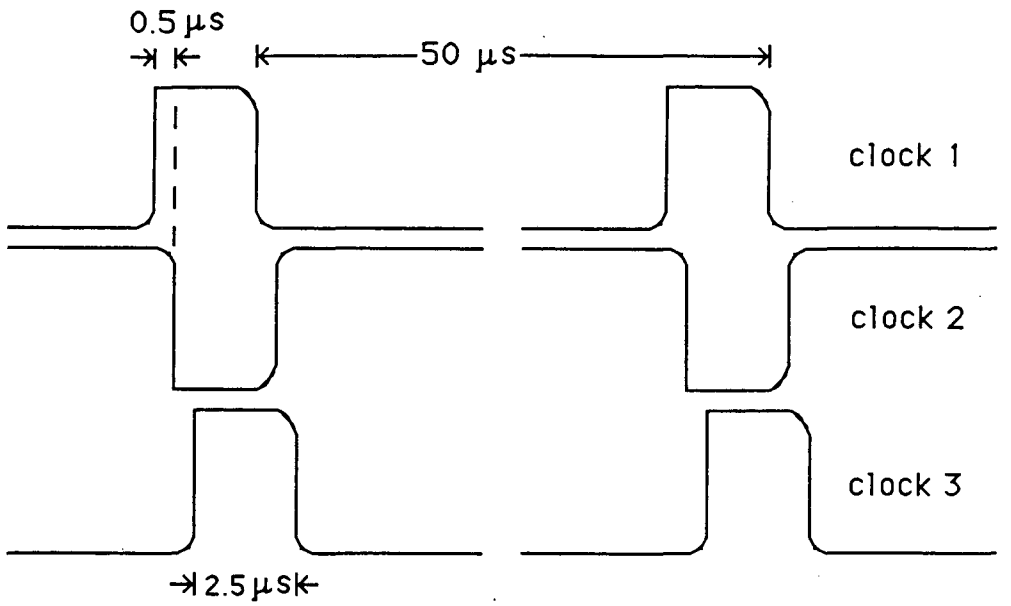

Figure 3.4 Phase diagram for the horizontal clocks.

night.) Before being sent to the CCD, the TTL levels from the timing circuit must be shaped and set to the proper voltages. Charge is transferred more efficiently if the clock pulses decay gradually. The decay time constant is about 0.5 µs for the horizontal clocks and 0.3 µs for the vertical clocks. The level of all the horizontal clocks is set to a low of -9.0 volts and a high of 0.7 volts. The vertical clocks swing from -10.0 to -0.5 volts. The horizontal levels are set higher than the vertical levels to improve charge transfer from the last image row to the horizontal register. Both the high and low voltage levels for each clock are independently adjustable although, in practice, the charge transfer and noise of the CCD are effected very little by changing these levels. Changing the horizontal and vertical clock voltages by as much as a volt has little effect as long as the horizontal levels are higher than the vertical levels.

3.2.2 Correlated Double Sampling

The first stage of amplification occurs on the CCD. Once a charge packet reaches the end of the horizontal register (see figure 3.5), it is dumped to a floating diffusion where the charge sets the gate voltage of the output FET. The floating diffusion is a diode with a large reverse bias so that when the last electrode goes to its low potential, all the charge below it is "pushed" onto the diode. When the floating diffusion receives the signal charge (q) its potential changes by a small amount $\Delta V = q / C$, where C is the effective capacitance of the floating diffusion. The charge is cleared from the floating diffusion when the reset clock (ϕ_r) swings from a low of -6.0 volts to a high of about 0.9 volts. This "opens" the gate of the reset FET and the charge is drawn from the floating diffusion to the reset drain (RD). When ϕ_r goes back to -6.0 volts, the gate closes and the floating diffusion is ready for the next pixel's charge.

The thermal noise on the floating diffusion can be estimated by using the fact that the thermal fluctuations in the energy stored in a capacitor is on the order of kT. Therefore,

$$q_{rms}^2 / 2C \sim kT.$$

The capacitance (C) of the floating diffusion is about 0.3 pf (or 2 electrons / μV), so the thermal noise (q_{rms}) on the capacitor at T = -100 °C is:

$$q_{rms} \approx (2 k T C)^{1/2} \approx 240 \text{ electrons.}$$

This noise is reduced by the technique of correlated double sampling (CDS). Figure 3.6 shows a circuit equivalent to the reset circuit. The switch and resistors

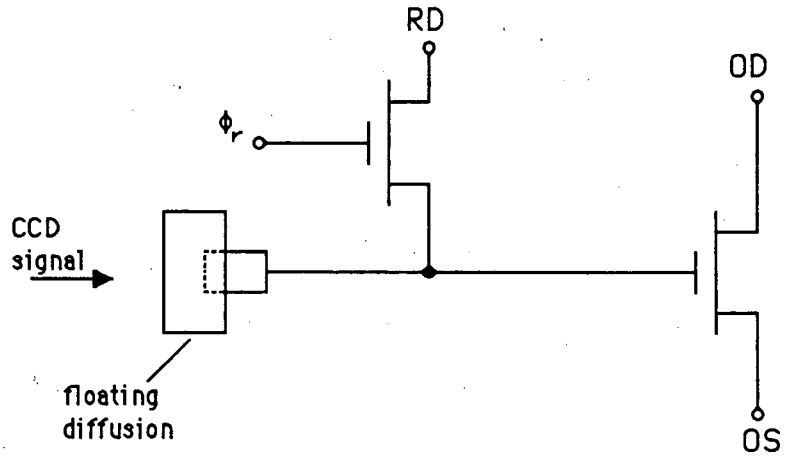

Figure 3.5 The CCD output stage and on-chip amplifier.

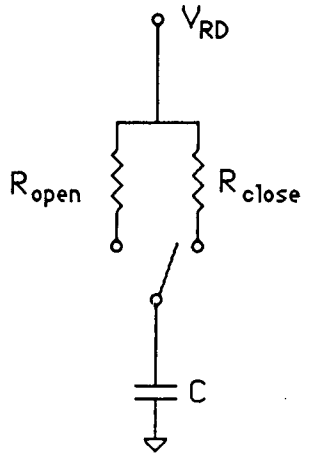

Figure 3.6 CCD reset equivalent circuit.

represent the reset FET and the capacitor represents the floating diffusion. When ϕ_r is high, the reset FET gate is open so the source to drain resistance is low (R_{open} is typically about $10^4\ \Omega$ for a MOSFET). When ϕ_r is low the gate is closed and the resistance is high ($R_{close} \approx 10^{12}\ \Omega$). Suppose that at t = 0, ϕ_r goes high to reset the capacitor and ready it for the next pixel's charge. The mean charge on the capacitor ($\overline{q}(t)$) is:

$$\overline{q}(t) = C\, V_{RD} \left(1 - e^{-t/\tau open} \right) + q_o$$

where, $\tau_{open} = R_{open}\, C \approx 10^{-6}$ ms and q_o is the charge from the previous pixel. The equation for the rms noise on the charging capacitor (q_{rms}) is derived in appendix II. The result is:

$$q_{rms}^2 = k\, T\, C \left(1 - e^{-2t/\tau open} \right).$$

The time scale over which the noise builds is 10^{-6} ms (τ_{open}). When the gate closes the time dependence is the same except that the time constant is $R_{close}\, C \approx 300$ ms. Correlated double sampling works by taking advantage of the this relatively long time constant. The output signal is sampled twice: once right after reset and once right after the charge is dumped to the floating diffusion. If the time between the two samples is much less than 300 ms then the noise will not have changed appreciably so the pixel charge can be recovered by subtracting the reset level from the signal level. In practice we use a time between samples of about 30 μs and so are able to virtually eliminate thermal noise.

3.2.3 CCD Signal Amplifiers

The output FET source (OS) is connected to the first stage of a preamplifier inside the vacuum housing (figure 3.7). This amplifier is an emitter follower and a

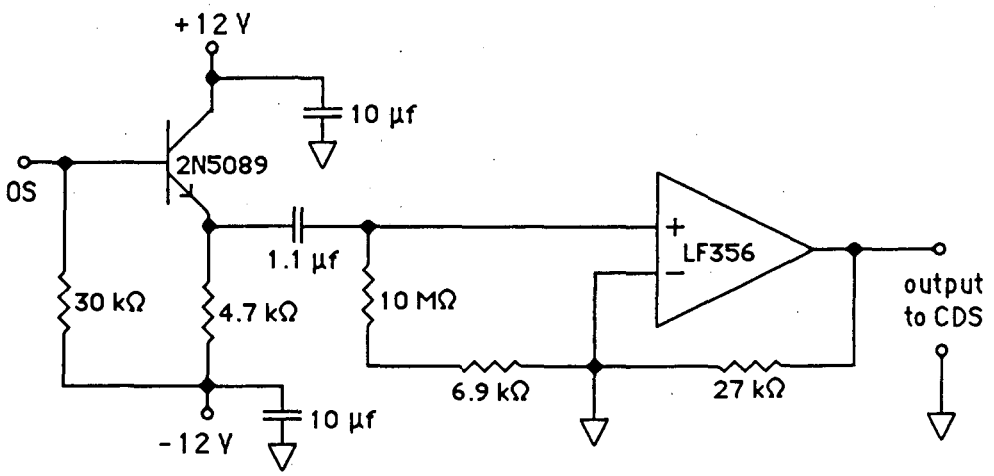

Figure 3.7 CCD preamplifier located inside the vacuum housing. OS is the output FET source (see figure 3.5).

noninverting op-amp with a gain of 5. The output of the preamp is connected to the amplifier and A/D converter by a twin-axial cable. The card cage amplifier consists of an integrating amplifier, two sample and hold chips and a 14 bit analog to digital converter (ADC). The clock signals required by the CDS amplifier are supplied by the same digital logic circuits that supply the CCD clock timing (§ 3.2.1). Four µs after the floating diffusion is reset, the integrating amplifier begins a 14 µs integration of the reset (noise) level. The integrated noise is then "stored" by a sample and hold. During the next 5 µs, the charge on the last element of the horizontal register is transferred to the floating diffusion. The signal is then integrated for another 14 µs and the resulting level (signal + noise) is stored by a second sample and hold. The reset level is "subtracted" from the signal level by a

differential amplifier whose output is then sent to the ADC where it is converted to the 14 bit serial signal fed to the computer (or stored on video tape).

3.3 CCD Performance

3.3.1 Dark Current

In a single pixel of a room temperature CCD, on the order of 10^6 electrons are generated per second. These thermally produced electrons constitute a "dark current" which will quickly saturate the CCD unless it is cooled or read out rapidly. CCDs used in commercial TV cameras are read out 30 times a second so thermal noise is not a problem. Our CCD must be cooled for the relatively long exposures we require.

We have found that some "hot" columns in our CCD have a higher dark current than others. Twenty to thirty columns become saturated after a five minute dark current integration at -80 °C. At -100 °C essentially all of the hot columns are gone. The only high dark current area left is the flare defect in the upper left hand corner. Except for this spot, which is ignored by all of the image processing software, the CCD has an average dark current of 20 electrons per second at -100 °C.

3.3.2 Gain and Readout Noise

Correlated double sampling reduces the output noise considerably (from 240 to 10-100 electrons rms) but does not eliminate it entirely. In order to estimate the

CCD output noise in electrons, the gain of the entire system (ie. the number of electrons per ADC unit) must be known. The simplest way to estimate it is to use the manufacturer's specification for the capacitance of the floating diffusion. A potential difference of 0.73 volts between the signal level and the reset level (measured at the preamp output) has been measured to give 1.0×10^4 ADC units. The gain of the preamp is 5 so the potential at OS is 0.15 volts. RCA claims the capacitance of the floating diffusion is about 0.3 pf or, in more convenient units, 2 electrons/μV. An estimate of the gain (G) can be obtained using these numbers.

$$G = (2 \text{ electrons}/\mu V) \times (0.15 \text{ V}) / (1.0 \times 10^4 \text{ ADU}) = 30 \text{ electrons/ADU}.$$

A more accurate technique of measuring the gain takes advantage of the fact that photoelectrons obey Poisson statistics (i.e. the variance of the distribution is equal to its mean). The signal, (S) in ADU, in a single pixel exposed to a fixed amount of light, is a sum of the contribution from photons and the contribution from the readout noise.

$$S = \gamma (N + n),$$

where γ is the inverse of the system gain G, N is the number of photoelectrons in the pixel, and n is the readout noise contribution to the signal measured in equivalent electrons. For several equivalent exposures the mean signal $\bar{S} = \gamma (\bar{N} + \bar{n})$. In the following, it is assumed that the *average* readout noise contribution ($\bar{n}$) is zero to simplify the algebra although carrying a nonzero value does not change the result. The variance in the signal (S_{rms}^2) over M exposures is:

$$S_{rms}^2 \equiv \sum (S_i - \bar{S})^2 / M = \gamma^2 \left[\sum (N_i - \bar{N})^2 / M + \sum n_i^2 / M - \sum (N_i - \bar{N}) n_i / M \right].$$

The first term in brackets is the variance of the photoelectron distribution, which is the mean number of photoelectrons. The second term is the variance of the readout noise (n_{rms}^2), and the last term is zero since the photoelectron and readout noise are uncorrelated. The above equation then simplifies to

$$S_{rms}^2 = \gamma^2 (\overline{N} + n_{rms}^2)$$

however, $\gamma \overline{N} = \overline{S}$ so

$$S_{rms}^2 = \gamma \overline{S} + (\gamma n_{rms})^2.$$

From the above equation, it is clear that if the signal variance is plotted versus the signal mean for many different exposure times, then the resulting plot should be a straight line whose slope is the inverse of the system gain and whose intercept gives the CCD readout noise.

Figure 3.8 shows S_{rms}^2 plotted against $\overline{S}$ for the CCD currently being used by the supernova search. The temperature of the CCD during the measurements was -103 °C. Each point was obtained by exposing the CCD to a constant light source (an LED) 10 times for a fixed amount of time. The Uniblitz shutter (§ 2.2) was used to vary the exposure time for the other points. The statistical error in S_{rms}^2 was estimated by taking the standard deviation of S_{rms}^2 over 25 pixels (the error bars shown in figure 3.8 are plus and minus one standard deviation). The slope of the line is 0.039 ± 0.007 ADU/photoelectron which gives a system gain, G = 25 ± 5 photoelectrons/ADU. This agrees reasonably well with the rough estimate calculated using the manufacturer's specification of the floating diffusion capacitance. The rms readout noise calculated from the intercept is 3.4 ± 0.4 ADU or 86 ± 15 electrons. John Geary (private communication) has tested many of the same model

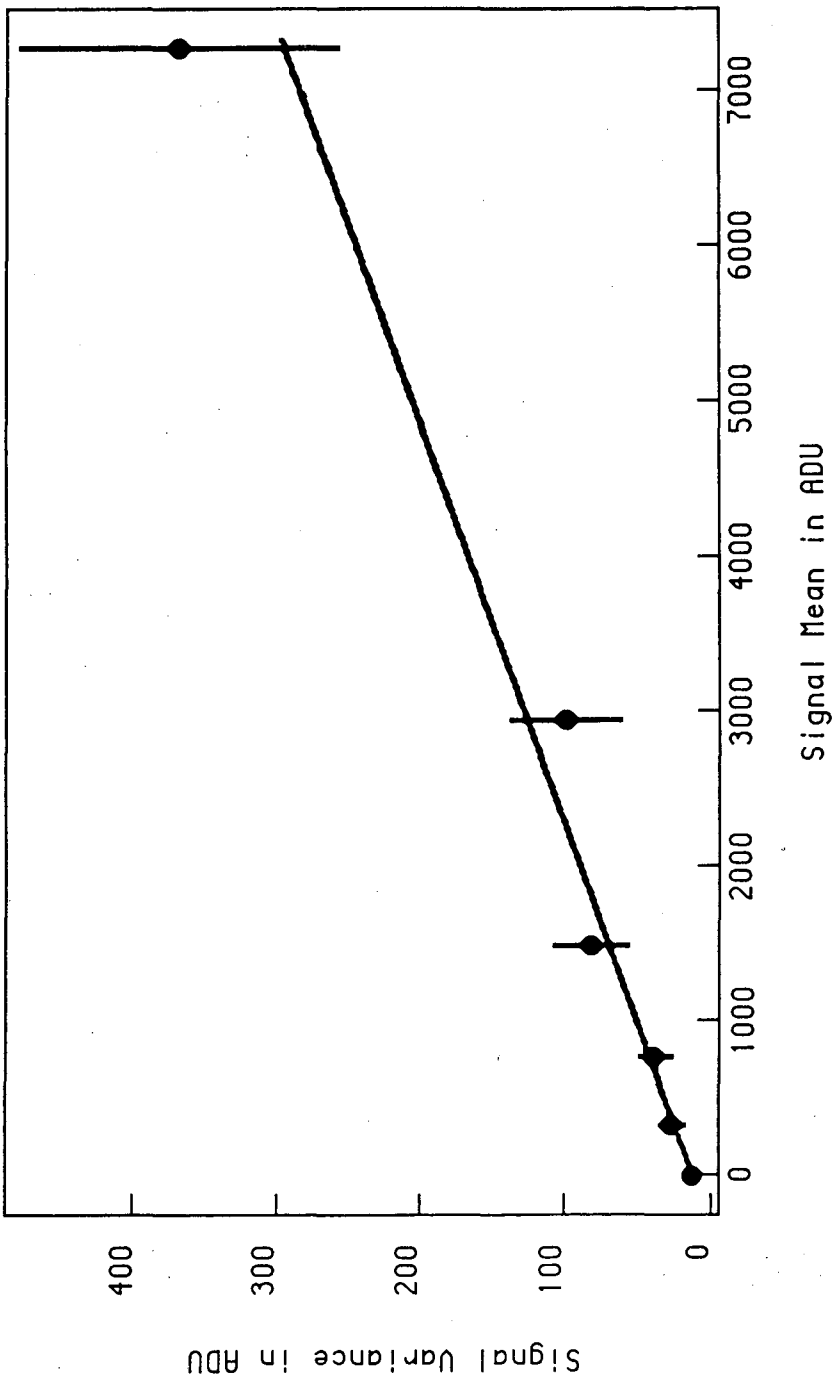

Figure 3.8 Plot of the signal mean versus the signal variance. These data were used to calibrate the CCD gain.

CCDs and has measured rms noise values anywhere from 50 to 120 electrons.

3.3.3 Transfer Efficiency

The first CCDs were surface channel devices with a pixel to pixel transfer efficiency (η) of only .990 (Beynon and Lamb 1980), so that after 100 transfers only about a third ($.990^{100} = .36$) of the initial charge was left in the pixel. Buried channel devices have a much better efficiency of from $\eta = .9995$ to .99995. The last pixel in a 512 by 320 CCD undergoes 832 transfers; even with a transfer efficiency of .99995, 4% of the original charge is left behind during transfer. However, the charge is not lost but is left behind in trailing pixels. In order to understand better how the charge is smeared by imperfect transfer, consider the one dimensional CCD diagramed in figure 3.9. If the initial charge in pixel 0 is Q and all the other pixels start out empty, then the charge left in pixel i (Q_i) after N transfers is

$$\frac{Q_i}{Q} = \frac{N!}{(N - i)!\, i!} (1 - \varepsilon)^i \varepsilon^{N-i}$$

where $\varepsilon = \eta - 1$ is the transfer *in*efficiency (Barbe 1975; Tans 1984). The amount of charge left in the original packet when it reaches the output gate (ie. after N transfers) is Q_N where

$$Q_N = (1 - \varepsilon)^N Q \approx (1 - N\varepsilon)\, Q, \qquad \text{for } N\varepsilon << 1.$$

This implies that the charge left in the CCD (Q_{OS}) is

$$Q_{OS} \approx 1 - (1 - N\varepsilon)\, Q = N\varepsilon Q = (1 - \eta) NQ.$$

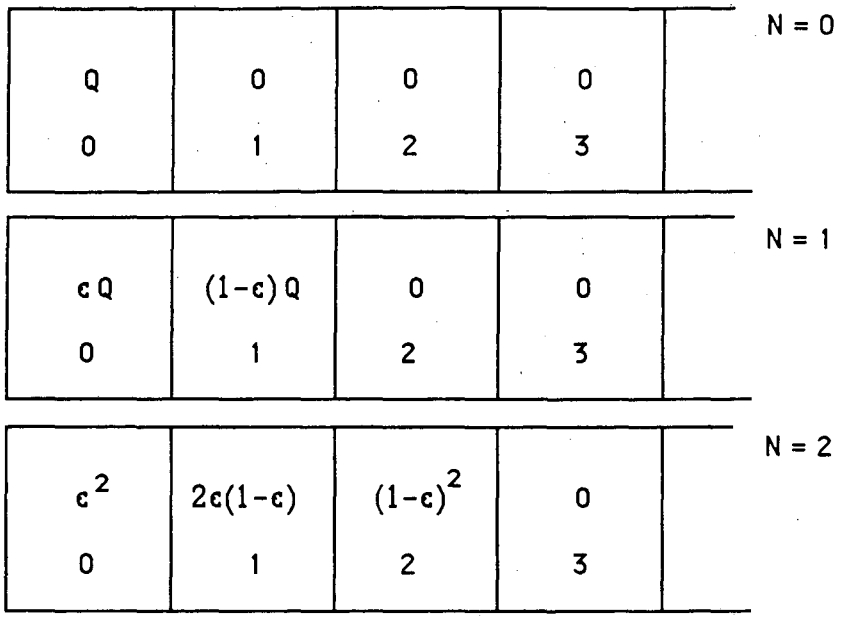

Figure 3.9 Charge transfer in a linear CCD. Q is the initial charge in pixel 0, ε is the transfer inefficiency, and N is the number of transfers.

Rearranging this equation gives an expression for the transfer efficiency in terms of the initial charge in pixel 0 and the amount of charge left in the CCD:

$$\eta = 1 - Q_{OS} / NQ.$$

This equations suggests that a simple way to measure the transfer efficiency is to overscan the CCD (ie. read it out as if it were a 356 by 1024 pixel array instead of 320 by 512) and sum the charge in the overscan region to get Q_{OS}. Both N and Q are known so the transfer efficiency (or inefficiency) is easily calculated.

Figure 3.10 shows a plot of transfer inefficiency versus CCD temperature. The transfer inefficiency was calculated for several rows and columns using the overscan technique outlined above. The row and column values were then averaged to give

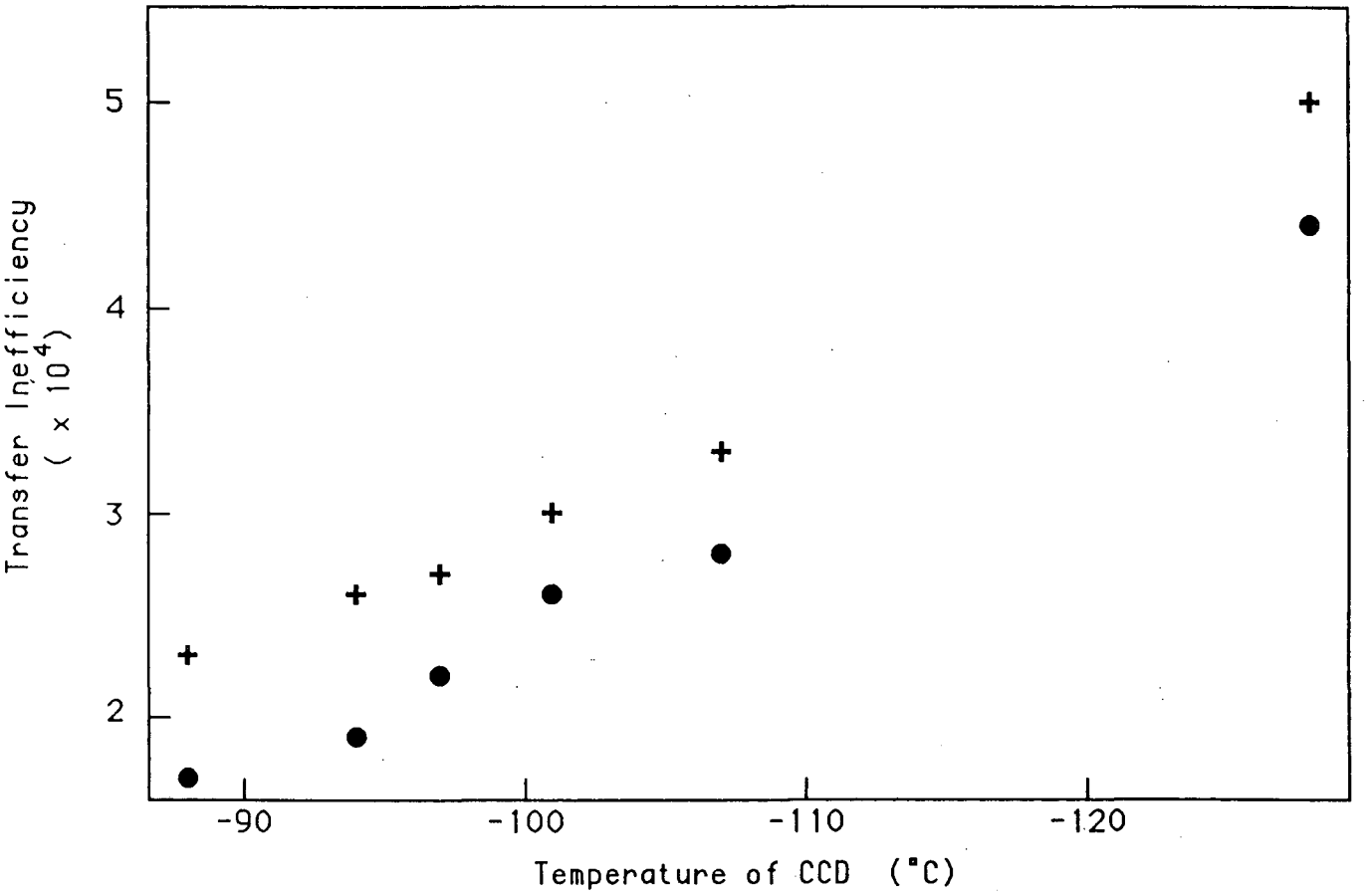

Figure 3.10 Transfer inefficiency as a function of temperature. The crosses represent the horizontal inefficiency; the dots represent vertical inefficiency.

the horizontal and vertical inefficiencies respectively. The horizontal inefficiency is somewhat larger than the vertical inefficiency. Both horizontal and vertical inefficiencies decrease as the temperature of the CCD is increased.

3.3.4 Quantum Efficiency

The manufacturer's specification for the quantum efficiency of the CCD model we are using is shown in figure 3.1. We have measured the quantum efficiency of our 'loaner' device at one wavelength (633 nm) by using a He-Ne laser whose power was determined with a calibrated photodiode. Figure 3.11 shows how the measurement was made.

Using the shortest exposure time possible with the Uniblitz shutter, the laser saturated the CCD. Two Melles Griot Precision Metallic neutral density filters were used to reduce the laser power into an acceptable range. The total attenuation of both filters is $10^{-6.89\pm0.05}$, at 663 nm. The filter closest to the CCD had an attenuation of $10^{-3.94\pm0.04}$, and the filter closest to the laser attenuated by a factor of $10^{-2.95\pm0.03}$. The laser spot on the CCD was about 100x100 pixels in size. The pin hole (~3 mm diameter) in the screen eliminated background light.

The photodiode gives $0.438\text{x}10^4$ volts/watt at λ=6328Å (manufacturer's calibration). The measured voltage across the photodiode when the laser was shining on it was 6.1-6.3 volts which gives 1.4 mW as the laser power. The number of photons/sec from the laser (N) is:

$$N = \text{power} \times \lambda / hc = (1.4 \times 10^{-3}\ \text{Watts})(6328\text{Å}) / hc = 4.6 \times 10^{15}\ \text{photons/sec.}$$

In order to get the number of photons expected at the CCD (n), N must be multiplied by a factor of .92 to correct for the attenuation of the quartz window in front of the CCD and by the filter attenuation ($10^{-6.89}$). Therefore,

$$n = (.92) \times (10^{-6.89 \pm 0.05}) \times N = (5.5 \pm 0.6) \times 10^{8}\ \text{photons/sec.}$$

The total brightness of the laser spot at the CCD is found by summing the number (ADU) in each pixel over the entire image, then subtracting the background. To get the total number of photoelectrons on the CCD, multiply this number by the gain of the system (25 photoelectrons/ADU). The results for a 0.5 and a 1 second exposure are shown in the table below.

exposure time	total ADU	number of photo-electrons/sec (n_{CCD})	quantum efficiency n_{CCD}/n
0.5 sec	3.78×10^6	$(1.9 \pm 0.4) \times 10^8$	0.31 ± 0.08
1.0 sec	7.48×10^6	$(1.9 \pm 0.4) \times 10^8$	0.31 ± 0.08

At 6328Å the CCD quantum efficiency is supposed to be almost 80%. This means the measured number is down by a factor of more than two. The most likely explanation for this is that the chip is thicker or thinner than specified so only some fraction of the photoelectrons are captured in the inversion region of each pixel (see Janesick, Elliott, and Blouke 1985). It must be remembered that this is a loaner chip and RCA would make no guarantee as to its performance.

The biggest problem with the current CCD is its poor quantum efficiency. Its low by a factor of two so all of our exposure times must be doubled to get the same supernova detection limit. It is hoped that the new CCD will remedy this problem. Several groups have measured the quantum efficiency of the newer model SID 501 chips and have found the quantum efficiency to be as good as RCA specified.

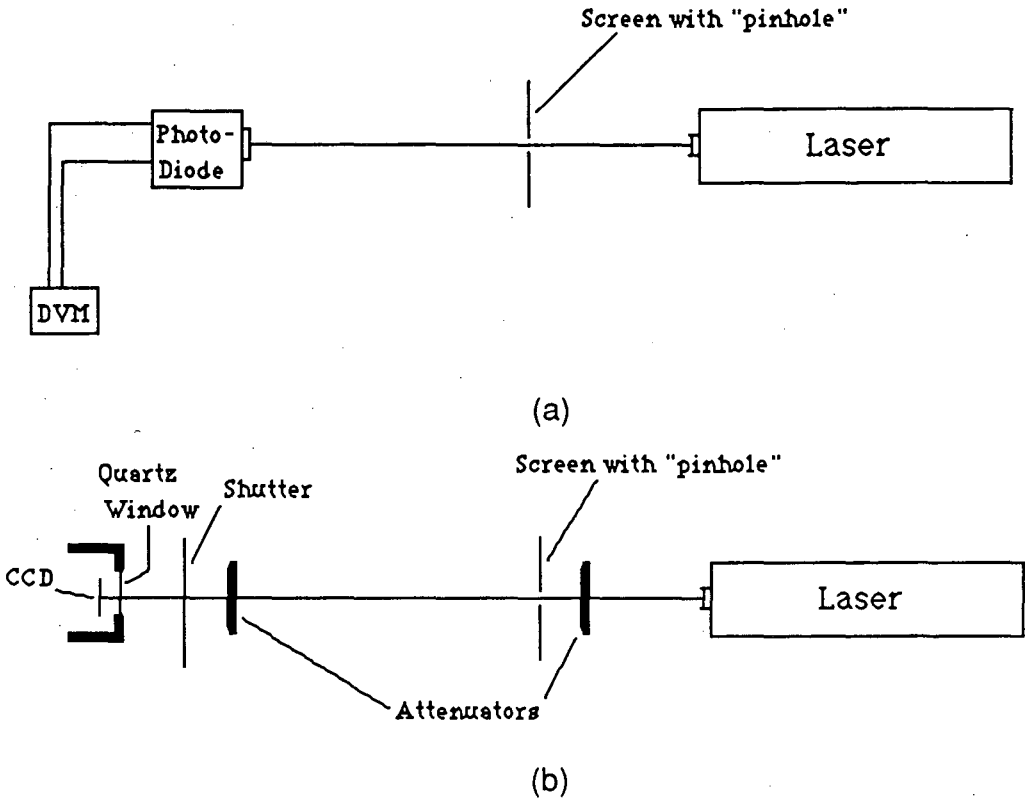

Figure 3.11 The apparatus used to calibrate the laser (a) and measure the CCD quantum efficiency (b).

4. Performance of Search System

4.1 Observation Strategy

4.1.1 Detection Limit

In order to get an estimate of our detection limit, we took several exposures of a standard star HD 114879 (spectral type A2) whose surface temperature is about 10,000 °K, which is the same as the temperature of a supernova at maximum light. The B magnitude of this star is 9.1 and all three exposure times were 5.0 seconds. Table 4.1 summarizes the results of these observations.

Date	Integrated Brightness (ADU)
09 July 1985	21467
"	21687
"	21578
"	21312
30 June 1985	20411
"	20783
"	20512
"	20764

Table 4.1 The brightness of the star HD 114879. The exposure time was 5.0 seconds. The integrated brightness is the background subtracted sum of the seven pixels around the brightest one.

The 3% difference in brightness on the two nights is probably due to differences in seeing and sky transmission. The average brightness from the night of June 30 will

be used in the example calculation below. The typical exposure time for a galaxy is 30 seconds and about 20% of the stars light falls in the brightest pixel, so a 30 second exposure of this star would yield about 2.5×10^4 ADU in the brightest pixel. The signal (S) expected from a 10,000° K star of B magnitude is

$$S = 2.5 \times 10^4 \cdot 10^{(9.1 - m) / 2.5} \quad \text{ADU.}$$

There are at least two contributions to the noise in the image: the CCD readout noise and the sky background noise. The sky background on the night of the observations was about 8.5 ADU/second = 210 pe^-/second/pixel so the noise contribution from the sky background $n_{sky} = (210\ t)^{1/2}$ where t is the exposure time. The CCD noise (n_{CCD}) is 86 electrons so the total noise (n) is

$$n = (n_{CCD}^2 + n_{sky}^2)^{1/2} = [\ 86^2 + (210)(30)\ ]^{1/2} = 120\ pe^- \approx 5\ \text{ADU.}$$

If our criterion for a supernova candidate is a signal to noise ratio of 5, then we are looking for a signal of 5n or 25. Using the above equation for the signal gives us the limiting magnitude for detection (m_{limit}).

$$m_{limit} = 9.1 + 2.5 \log(2.5 \times 10^4 / 25) = 16.6.$$

The absolute B magnitude of Type I and Type II SN at maximum light is -19.7 and -19.0 respectively (§ 1.1). At 50% of maximum light their magnitudes are -18.9 for Type I and -18.2 for Type II. The maximum distance D at which we could see SN at 50% of maximum is given by the equation:

$$D = 10^{-5} \cdot 10^{(m_{limit} - B_{50\%})/5} \quad \text{Mpc.}$$

Table 4.2 shows the distance at which we can find both Type I and Type II SN at

50% of maximum light. The distance is shown in Mpc, velocity ($v = H_0 D$) and redshift ($z = v/c$). A Hubble constant of $H_0 = 50$ km/sec/Mpc has been used in all of the above calculations.

	Distance (D)	v	z
Type I	125 Mpc	6250 km/sec.	0.020
Type II	91 Mpc	4560 km/sec.	0.015

Table 4.2 The maximum distance, velocity and redshift at which we can currently detect supernova at 50% of maximum luminosity.

Note that the calculations above used only the brightest pixel of the star image for calculation. This is only about 20% of the star's light. This implies that a better detection limit might be achieved by summing over several pixels.

4.1.2 Galaxy Selection

The galaxies to be searched are selected from the galaxy sky block files described in Appendix I. The skyblock files were generated from the "redshift" catalogue compiled by Huchra and Davis. This catalog lists 14401 galaxies, and is available on magnetic tape. The listing contains the name of the galaxy, its coordinates, integrated brightness, velocity, and its morphological type. We only include galaxies in the observations list whose velocities are less than 6000 km/second and whose integrated magnitudes are less than 16. The velocity cut ensures that if we search the galaxies frequently we will find the SN in these

galaxies at or before they reach 50% of maximum brightness. The cut at 16 magnitude rules out only a small fraction of the galaxies that pass the velocity cut. This cut was instituted because it was found that when building the reference images, it was impossible confidently to identify the galaxy in the two minute reference exposures if they were dimmer than 16. There are about 5500 galaxies in the redshift catalog that pass these cuts and are visible from the Leuschner Observatory.

4.2 Speed of Observations

Telescope time is being split between collecting more reference images and searching. After we have acquired about 1500 galaxy reference images (as of November 1985 about 1000 galaxies had been observed and built), we will begin searching almost full time; the rest of the time will be spent on collecting enough new reference images to make up for the reference galaxies that are no longer visible at night. On the average it takes about 45 seconds to acquire a search image, so on a typical night about 500 galaxies can be observed. Acquiring reference images takes longer because of the two minute exposure time, so about 200 references can be observed per night. The exposure time for search images is 30 seconds. It only takes about 15 seconds to move the telescope and read the CCD. Ten seconds of this time is used to send the pointing information across the phone line (the CCD is read out during these communications) and it takes about 5 seconds to move from one galaxy to the next (the distance between galaxies is typically less than 5 degrees). One obvious way to speed the telescope is to eliminate the 300 baud communications between the computers. A program is being written on the telescope computer to allow it to run the observations from a file transferred to it

during the day. In principal this could eliminate a few seconds from each observation cycle, but the modem signal is recorded on the audio track to keep track of what is on video tape. One solution to this problem is to have the telescope computer transmit a minimum of information (a single number) out to a modem whose signal is recorded in the usual way.

5. Observations of the Supernova in NGC 5033

On June 13, 1985, N. Metlova of the Crimean Observatory discovered a supernova in NGC 5033 (IAU Circular No. 4077). He estimated its photographic magnitude to be 12.5 on the date of discovery. This supernova provided us with the opportunity to see how well we could perform photometry with the CCD. We started observing this supernova on June 25, 1985 and were able to followed it until it was no longer visible in the night sky. Figure 5.1 shows a CCD image of this supernova taken by us on July 9, 1985.

The observations were performed in the usual automated mode. An observation list was made which contained two 5.0 second exposures of a standard star followed by three exposures of the galaxy (two 30 second and one 3 minute exposure), then another two 5.0 second exposures of the standard. The standard star HD 114879 is a spectral class A2 star whose temperature (~9730 °K) is about the same as the temperature of a supernova at maximum luminosity. The integrated brightness of each object was found by summing the background subtracted values of a 7 by 7 block of pixels centered on the object's brightest pixel. The background was estimated by averaging the pixel values of four 3 by 3 blocks, one block starting at each corner of the 7 by 7 block. The magnitude of the supernova (m_{SN}) was found by using the equation:

$$m_{SN} = m_{HD} - \log(SN/HD),$$

where, $m_{HD} = 8.95$ is the visual magnitude of the standard star and SN is the integrated brightness of the supernova. HD is found by averaging the standard's integrated brightness over the four exposures taken each night. Table 5.1 summarizes the results of the observations.

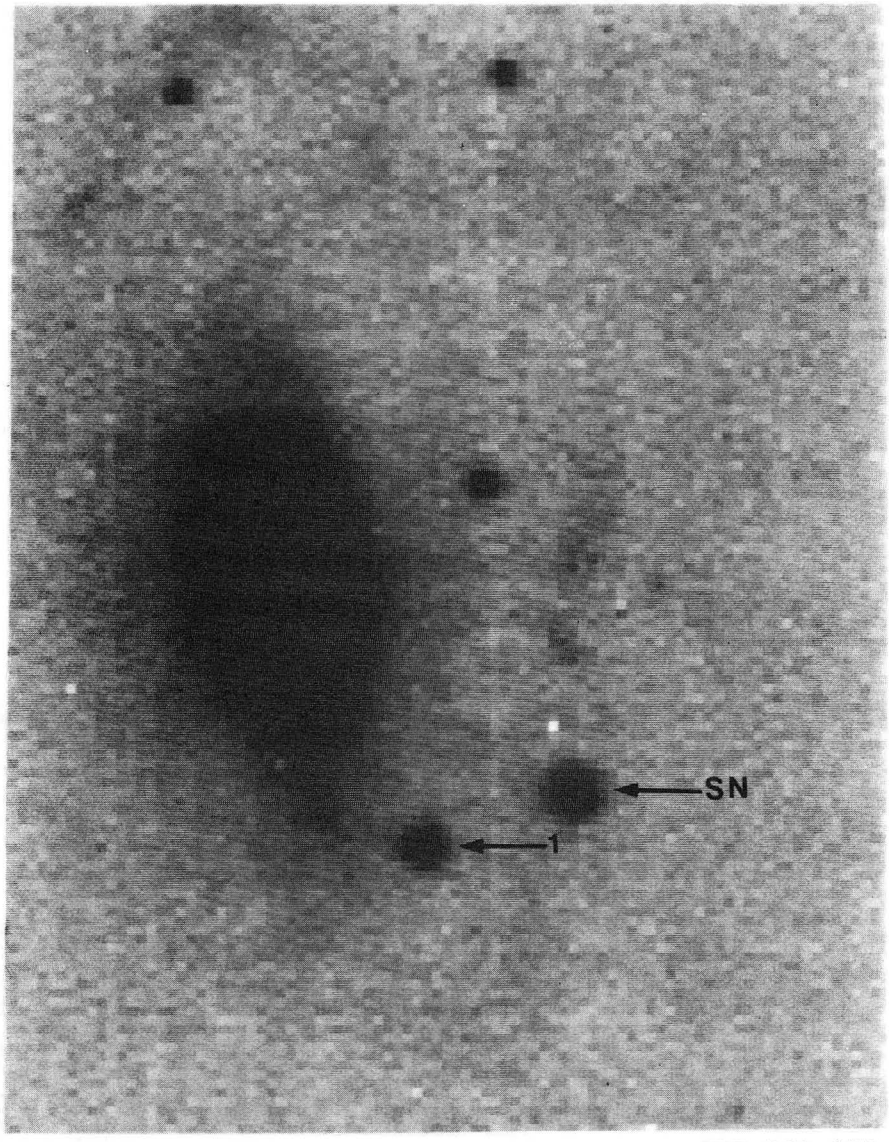

XBB 861-455

Figure 5.1 CCD image of NGC 5033. The supernova and the first monitor star are shown. The second monitor star is not visible in this enlargement.

Date	m_{SN}	m_1	m_2
June 25, 1985	12.81	14.16	13.71
June 30, 1985	12.85	14.08	13.65
July 9, 1985	13.12	14.13	13.76
July 10, 1985	13.13	14.15	13.77
July 18, 1985	13.27	14.15	13.64
July 25, 1985	13.40	14.17	13.67
Aug. 1, 1985	13.55	14.11	13.73
Average	--	14.14 ± 0.03	13.70 ± 0.05

Table 5.1 Summary of observations of the supernova in NGC 5033. m_{SN} is the magnitude of the supernova, m_1 is the magnitude of the first monitor star, and m_2 is the magnitude of the second monitor star.

The standard deviation of m_1 and m_2 is averaged and used to estimate the uncertainty in m_{SN} to be about 0.04 magnitudes. Figure 5.2 shows a plot of m_{SN} as a function of time. The relative error in the magnitude is only 0.4% which translates to an error in the supernova's estimated flux of about 5%. However, the CCD has not been calibrated to any standard photometric system and the spectral response of the detector is unknown. More work must be done in order to compare these measurments with other SN observations. For the early part of the light curve, the supernova magnitudes quoted are probably very close to being visual magnitudes since the reference star was chosen to have about the same temperature (and hence the same continuum spectrum) as a supernova near maximum light. In the later part of the light curve, the supernova has probably cooled enough to make the difference in the reference star and supernova continuums significant.

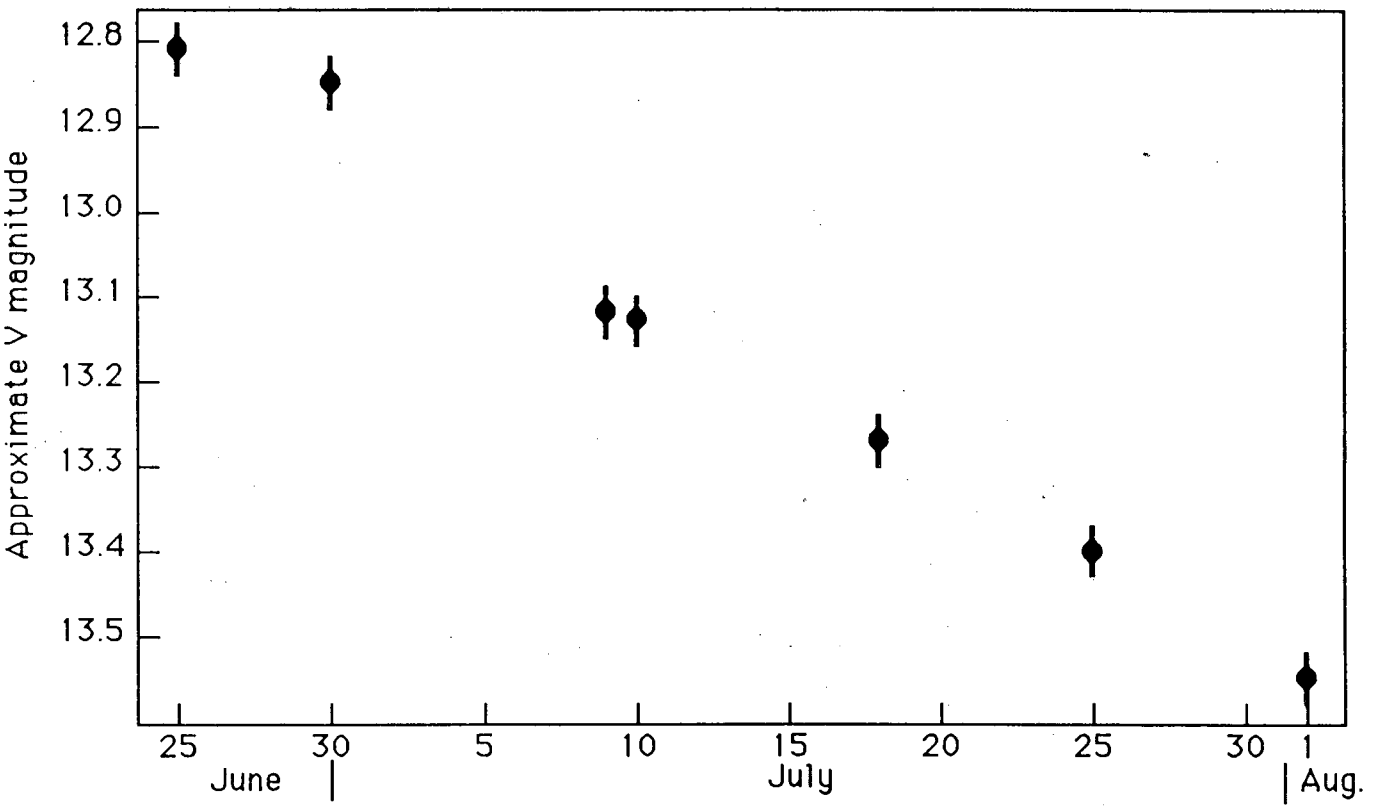

Figure 5.2 Light curve of the supernova in NGC 5033.

6. Conclusion

Observations of 1500 galaxies weekly will result in finding at least one supernova per month. This will more than double the number of supernovae currently found each year. All of the supernovae discovered by the Berkeley search will be found at or before maximum luminosity, so in less than a year the search will also almost double the total number of supernova observed before maximum light. However, an even larger number of observations would allow better estimates of supernova rates and the uniformity of Type I light curves. One of the immediate goals of the Berkeley search is to speed up the observations so that as many as 2500 galaxies can be scanned each night (6000 galaxies on a three night cycle). This would give a detection rate of about one supernova per week.

If 2500 galaxies are to be observed in a single night then only about 10 seconds can be spent acquiring each image. Currently, about 2/3 of the time on each galaxy is spent exposing the CCD. Several things are being done to reduce the exposure time. A new CCD (RCA model SID 501) is being developed which should have twice the quantum efficiency and about half the readout noise of the CCD now in use. If detector noise dominates, then with the new CCD, the same signal to noise ratio can be achieved in 1/4 of the time. The exposure time can be further reduced by using a telescope with a larger collecting area. The Monterey Institute for Research in Astronomy (MIRA) has a 36 inch telescope which was used in the early stages of the supernova search. This telescope has 1.4 times the collecting area of the Leuschner telescope and is located at an excellent observing site on Chew's Ridge near Carmel California. (The MIRA site has much better sky transmission and seeing than the Leuschner site.) At Leuschner, about half of the incoming light is

lost in the reduction optics. The MIRA telescope has a different plate scale so a simpler reduction scheme with better transmission could be used (Kare 1984). An exposure time of about 5 seconds is not unreasonable if all of the above improvements are implemented. The next most time consuming part of each observation is the 8 seconds it takes to read the CCD (the telescope can be moved while the CCD is reading out). This time can be cut in half by replacing the 2 Mhz clocking crystal with a 4 Mhz crystal.

As far as the observational part of the program is concerned, a speed of 10 seconds per observation is achievable. In order to perform real time analysis of each image, the image processing software must also be sped up. The RSX 11-M operating system allows multitasking so that image analysis can continue while the CCD is being read and while the previous image is being processed. If half of each image cycle is taken up by non-CPU intensive tasks like disc access and direct memory access (DMA), then two image cycles can be run simultaneously without slowing the image processing of either. Allowing two image cycles to run simultaneously would allow each to take an average of about 20 seconds. The actual time required for each cycle depends on the number of pixels in each image whose value is more than our threshold of five standard deviations above the background level. Currently the image processing program takes longer than 20 seconds, but little of the code has been optimized for speed. Minimizing disc I/O and coding critical parts of the routines in the DEC assembly language (MACRO) should speed the image cycle considerably.

Accurate light curves and supernova rates can be achieved easily with the search

system. Observations of the supernova in NGC 5033 demonstrate that the CCD system can be used to perfom photometry that is accurate to about 5 percent (§ 5.), although the detector needs to be calibrated to a standard photometric system (eg. the Johnson UBV system) to make these measurments meaningful. The average supernova rate can be obtained directly from the detection rate, and with a little work the rates as a function of morphological type and position within the galaxy can be obtained. These observations, as well as follow up observations on larger telescopes, will make a significant contribution to our understanding of supernovae.

Appendix I -- Galaxy Sky Block Files

The galaxy sky block files contain a list of the galaxies we will observe in the near future. Each file contains a list of all the galaxies in a block of sky one hour of right ascension wide by ten degrees of declination long. The first character of the name is 'B', the second two characters give the starting right ascension of the block. The next character is 'P' if declination > 0 and 'M' if declination < 0 and the last character specifies the starting declination. The UIC for these files is [300,316] and the extension is .GBL. The file named '[300,316]B12P1.GBL', for example, contains all the galaxies between 12 and 13 hours right ascension and from +10 to +20 degrees of declination. Shown below is a section of the galaxy sky block file B12P1.

B12P1	1	N4048	12	0	18.0	18	17	0.0	50	14.4	4777	0
B12P1	2	N4049	12	0	24.0	19	2	0.0	50	14.2	839	0
B12P1	3	1200+1647	12	0	48.0	16	47	0.0	50	14.6	6938	0
B12P1	4	1200+1646	12	0	54.0	16	46	0.0	50	14.0	4048	0
B12P1	5	N4067	12	1	36.0	11	8	0.0	50	13.2	2403	0
B12P1	6	N4064	12	1	36.0	18	43	0.0	50	12.6	1033	0
B12P1	7	N4078	12	2	12.0	10	52	0.0	50	13.9	2529	0
B12P1	8	1202+1809	12	2	48.0	18	9	0.0	50	14.1	4378	0
B12P1	9	1202+1812	12	2	48.0	18	12	0.0	50	14.6	4248	0
B12P1	10	1204+1716	12	4	36.0	17	16	0.0	50	16.0	6740	0
B12P1	11	I3008	12	5	24.0	13	50	0.0	50	15.0	6947	0
B12P1	12	1205+1130	12	5	30.0	11	30	0.0	50	15.3	9523	0
B12P1	13	N4124	12	5	36.0	10	40	0.0	50	12.7	1674	0
B12P1	14	1205+1357	12	5	48.0	13	57	0.0	50	15.3	2275	0

The first set of characters is the sky block name; next comes the number of the galaxy in that block. The next field of characters is the 'name' of the galaxy, i.e. its NGC number or an identifier from some other catalog. The next two sets of three numbers each are the right ascension and declination respectively. The next number is the epoch of the coordinates (50 means 1950). The visual magnitude of the galaxy is next and after that comes the velocity in km/sec. Last is the flag specifying the status of the galaxy. Zero means the galaxy does not yet have a reference image built; a 1 means the reference is built and the galaxy should be put on a search list. A 2 means the galaxy has been observed, but no reference image has been built.

Appendix II -- Thermal noise on a Charging Capacitor*

Consider the RC circuit shown in the figure below. The dotted line represents the effective circuit of a resistor which consists of a Johnson noise generating signal source and a 'perfect' resistor of resistance R.

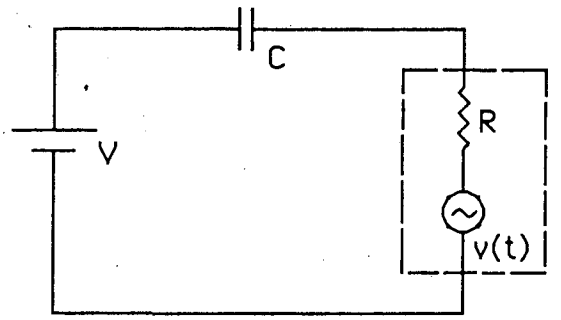

Summing the voltages around the circuit gives the equation:

$$IR + Q/C = V + v(t)$$

or,

$$\frac{dQ}{dt} + \frac{Q}{CR} = \frac{V}{R} + \frac{v(t)}{R}.$$

This can be rewritten as

$$\frac{d}{dt}(Q\, e^{t/RC}) = \frac{1}{R}\ (V + v(t))\, e^{t/RC}.$$

The solution to this equation is

$$Q(t) = VC\,(1 - e^{-t/RC}) + e^{-t/RC} \int_0^t v(t)\, e^{\tau/RC}\, d\tau / R.$$

The Johnson noise is random and therefore averages to zero so, the average charge on the capacitor $< Q(t) >$ is given by

$$< Q(t) > = VC\,(1 - e^{-t/RC}).$$

The rms squared charge on the capacitor is

$$Q_{rms}^{\,2} = < (Q(t) - < Q(t) >)^2 > = e^{-2t/RC} < (\int v(\tau)\, e^{\tau/RC}\, d\tau)^2 > / R^2.$$

which reduces to

$$Q_{rms}^{\,2} = e^{-2t/RC} \int\int < v(\tau)\, v(\tau') > e^{(\tau + \tau')/RC}\, d\tau\, d\tau' / R^2.$$

If v(t) is the Johnson noise of the resistor, then

$$< v(\tau)\, v(\tau') > = 4kTR\delta(\tau - \tau').$$

Substituting this in the equation for Q_{rms}, allows us to perform the integration. The result is

$$Q_{rms} = [\, 2kTC\,(1 - e^{-2t/RC})\,]^{1/2}.$$

* This derivation is adapted from Barbe 1975.

References

Arnett, W. D., D. Branch, and J. C. Wheeler, 1985, Nature **314**, 337.

Axelrod, T. S., 1980, in *Type I Supernovae*, edited by J. C. Wheeler (University of Texas, Austin, and MacDonald Observatory), p.80.

Barbe, D.F., 1975, Proceedings of the IEEE, Vol. 63, No. 1.

Bethe, H. A., G. E. Brown, J. Cooperstein, and J. R. Wilson, 1983, Nucl. Phys. **A403**, 625.

Beynon, J. D. E. and D. R. Lamb, 1980, *Charge Coupled Devices and Their Applications* (McGraw Hill).

Branch, D., 1982, in *Supernovae: A Survey of Current Research*, edited by M. J. Reese and R. J. Stoneham (D. Reidel, Dordrecht), p. 267.

Burbidge, E. M., G. R. Burbidge, W. A. Fowler, and F. Hoyle, 1957, Rev. Mod. Phys. **29**, 547.

Colgate, S. A. and C. McKee, 1969, Ap. J. **157**, 623.

Culver, J., 1982, *A CCD Camera for an Automated Supernova Search*, Senior Honors Thesis (University of California, Berkeley).

Graham, J. R., W. P. S. Meikle, D. A. Allen, A. J. Longmore, and P. M. Williams, 1985, preprint.

Hillebrandt, W., K. Nomoto, and R. G. Wolff, 1984, Astron. Astrophys. **133**, 175.

Iben, I. Jr., and A. V. Tutukov, 1984, Ap. J. Suppl. Ser. **54**, 335.

Janesick, J., T. Elliott, T. Daud, and J. McCarthy, 1985, preprint.

Kare, J. T., C. R. Penneypacker, R. A. Muller, T. S. Mast, F. S. Crawford, and M. S. Burns, 1982, in *Supernovae: A Survey of Current Research*, edited by M. J. Reese and R. J. Stoneham (D. Reidel, Dordrecht), p. 325.

Kare, J. T., 1984, Ph.D. thesis (University of California, Berkeley; Report No. LBL-19340).

Niemela, V. S., M. T. Ruiz, and M. M. Phillips, 1985, Ap. J. **289**, 52.

Nomoto, K., 1982, in *Supernovae: A Survey of Current Research*, edited by M. J. Reese and R. J. Stoneham (D. Reidel, Dordrecht), p. 205.

Tammann, G. A., 1982, in *Supernovae: A Survey of Current Research*, edited by M. J. Reese and R. J. Stoneham (D. Reidel, Dordrecht), p. 371.

Tans. P., 1985, private communication.

Treffers, R. R., 1985, preprint.

Weaver, T., S. E. Woosley, and G. M. Fuller, 1985, in *Numerical Astrophysics*, edited by J. Centrella, J. LeBlanc, and R. Bowers (Jones and Bartlett, Boston), p. 422.

Wilson, J. R., R. Mayle, S. E. Woosley, and T. Weaver, 1985, preprint.

LAWRENCE BERKELEY LABORATORY
TECHNICAL INFORMATION DEPARTMENT
UNIVERSITY OF CALIFORNIA
BERKELEY, CALIFORNIA 94720